REPORT OF INVESTIGATIONS/1988

# Causes and Control of Coal Mine Bumps

By K. Y. Haramy and J. P. McDonnell



BUREAU OF MINES

UNITED STATES DEPARTMENT OF THE INTERIOR

Report of Investigations 9225

# Causes and Control of Coal Mine Bumps

By K. Y. Haramy and J. P. McDonnell

UNITED STATES DEPARTMENT OF THE INTERIOR
Donald Paul Hodel, Secretary

BUREAU OF MINES
T S Ary, Director

**Library of Congress Cataloging in Publication Data**

**Haramy, Khamis Y.**
Causes and control of coal mine bumps.

(Bureau of Mines report of investigations; 9225)

Bibliography: p. 34.

Supt. of Docs. no.: I 28.23:9225

1. Coal mines and mining—Accidents. 2. Rock bursts. I. McDonnell, John P. II. Title. III. Series: Report of investigations (United States. Bureau of Mines); 9225

TN23.U43 TN311 622 s 622'.8 88-600223

# CONTENTS



## ILLUSTRATIONS

## ILLUSTRATIONS—Continued



## TABLES



## UNIT OF MEASURE ABBREVIATIONS USED IN THIS REPORT

| | | | |
|---|---|---|---|
| Btu | British thermal unit | lb | pound |
| Btu/s | British thermal unit per second | lb·ft | pound per foot |
| dB | decibel | lb·ft$^3$/min | pound per cubic foot per minute |
| deg | degree | m | meter |
| ft | foot | MHz | megahertz |
| ft/ft | foot per foot | min | minute |
| ft/min | foot per minute | mm | millimeter |
| gal | gallon | MPa | megapascal |
| gal/min | gallon per minute | pct | percent |
| h | hour | psi | pound per square inch |
| Hz | hertz | psi/d | pound per square inch per day |
| in | inch | psi/ft | pound per square inch per foot |
| in$^2$ | square inch | rpm | revolution per minute |
| J | joule | ton | ton |
| kHz | kilohertz | | |

# CAUSES AND CONTROL OF COAL MINE BUMPS

By K. Y. Haramy, [1] and J. P. McDonnell [1]

## ABSTRACT

Coal mine bumps involve the violent, rapid failure of coal and rock around a mine excavation. Deep coal mines with strong roof and floor rocks and high-stress conditions frequently experience face and rib bumps. The bump problem is becoming more severe as mining depth increases, prompting efforts to control high stress in advance of mining.

This Bureau of Mines report presents a review of the most widely used methods to detect and destress high-stress zones along coal faces and an investigation of stress-related bump problems and destressing techniques at a cooperating mine. Geotechnical instrumentation and microseismic methods were used to better understand bump occurrences in underground coal mines. Laboratory tests of the drilling-yield method for high-stress detection were conducted to determine the correlation between the volume of cuttings obtained and the magnitude of the applied stress at various confining pressures. A three-dimensional, multiple-seam computer modeling program, MULSIM, was used to evaluate the effectiveness of stress-relief methods.

Modeling results indicate that dangerously high-stress areas can be controlled by either proper planning or destressing. Proper mine planning guidelines and destressing methods such as volley firing, hydraulic fracturing, and auger drilling are discussed.

[1] Mining engineer, Denver Research Center, Bureau of Mines, Denver, CO.

## INTRODUCTION

Coal bounces, bumps, and outbursts are major hazards to underground coal mining in many parts of the world. These events have the potential to inflict severe injury to mining personnel. Invariably, production is disrupted, and mine closure may be required. Although such events have been common to coal mining for many years, confusion still exists regarding their definitions. At the Bureau of Mines, these events are defined as follows: a bounce is a sudden forceful impact or vibration felt in the mine, which may be accompanied by face or rib sloughage and/or pillar and roof separation; a bump is an instantaneous release of roof, rib, or floor material propelled into a mine opening; an outburst is a bump that is accompanied by rapid release of a large volume of gases.

Mine Safety and Health Administration (MSHA) statistics from U.S. underground coal mines reveal that, between 1978 and 1984, 73 accidents were attributed to bumps and outbursts. The number of actual bump accidents is probably much higher. For example, a bump or an outburst may trigger explosions and contribute to other ground control problems. These events are not reported as bumps, but rather as an explosion, floor heave, or roof fall. Consequently, accurate documentation on accidents caused by these occurrences is unavailable.

It is a well-known fact that the severity and frequency of bumps increase with depth. The cause of this increase is usually attributed to the increasing weight of the overlying strata and the increasing stress in the rock strata with depth. However, depth is not the only factor that can contribute to bumps. Bumps have been reported in mines under only 1,000 ft of cover. In general, bumps in shallow mines occur infrequently and are not as severe. In most deep mines that are bump prone, the depth at which bumps are first experienced is usually below 2,000 ft; in most instances, they become a serious problem after 3,000 ft. However, some mines have operated at depths of greater than 5,000 ft without bumps. This indicates that site-specific conditions other than depth are also important factors.

The majority of the U.S. coal reserves are in the West, and production from western seams is projected to increase dramatically. Unfortunately, most of the Western U.S. reserves are deep and steeply dipping, often having thick, massive sandstone layers in close proximity to the seam, and therefore may be more prone to bumps.

Recognizing the bump problem in deep western coal mines, and in an attempt to allow future coal production under safer conditions, the Bureau initiated long-range research programs to develop technology for proper mine planning and stress control to prevent bumps. The research was conducted under an in-house project entitled "Research on the Initiation, Monitoring, and Destressing of Coal Mine Bounces, Coal Bursts, and Gas Outbursts in Deep Western Mines." The project reported here examined the different factors affecting bump conditions, different methods of detecting bump-prone areas, and the methods used to control potential bump conditions. Also described is an analysis of the causes of major bumps in a deep western coal mine.

## BUMP CLASSIFICATIONS

Bumps have been classified in a variety of ways, depending on the country, mine, and nature of occurrence. After an extensive study conducted by Phillips (*1-2*),[2] coal mine bumps were categorized as either pressure or shock bumps. A pressure bump occurs when a strong or brittle pillar in a developed area is statically stressed past the failure strength of the coal. A shock bump is caused by dynamic loading of the coal through either dramatic changes in the stress distribution within the overlying strata or by an abrupt loading of the coal seam ahead of the face resulting from dynamic roof rock failure. Holland (*3*) noted that the majority of bumps classified as shock bumps actually occurred in areas within the mine where the coal was already subjected to high levels of static loads. His study also concluded that bumps previously thought to be caused by dynamic loading were actually the result of either local variation in mine geology and coal properties, or improper mine design and sequencing, which created zones of high stress.

In Poland, (*4*) bumps are classified as either seam, roof, or floor bumps, depending on the area of failure. In the Republic of South Africa, (*5*) rock bumps are classified as ring, shear, or pillar bumps, depending on the stress and failure mechanism.

## BUMP MECHANISMS AND CONTRIBUTING FACTORS

Many studies have been conducted to understand the causes of bumps and outbursts and to predict their occurrence. The exact causes of bumps and outbursts are very difficult to determine, and reliable prediction is nearly impossible. While localized high-stress zones are common to all bump and outburst occurrences, other factors may act independently or together to cause a bump. The contributing factors shown in figure 1 are combined under four major categories: strain energy, geologic characteristics, mine design, and physical properties.

### STRAIN ENERGY

Coal has the capacity to store large amounts of strain energy before failing. The total energy stored depends on the coal, roof, and floor material properties, lateral confinement, and the magnitude of the applied stress. Before mining, the roof, coal seam, and floor are in equilibrium. Entry development redistributes stresses in the rock mass and results in permanent deformation around the opening. Stress increases around the opening until a critical level is reached; the capacity of the coal to store strain energy is reached, and any additional stress will cause the coal to bump (*6*).

[2] Italicized numbers in parentheses refer to items in the list of references preceding the appendix at the end of this report.

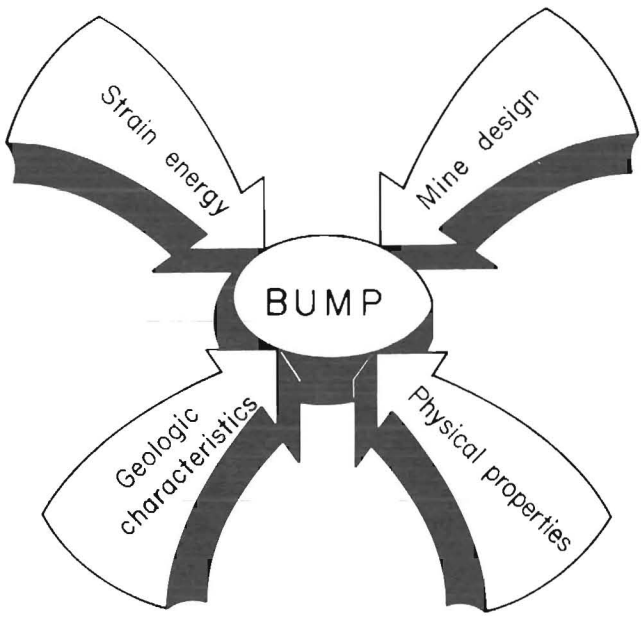


Figure 1.—Factors affecting coal mine bumps.

An energy index obtained from laboratory-derived stress-strain curves can be used to estimate the ability of coal to bump. Figure 2 shows typical loading and unloading curves for laboratory samples. The area under the unloading curve is termed $A'_e$. The area between the loading and unloading curves is termed $A_e$, and the energy index is a comparison of the two areas, $A'_e$ and $A_e$, and can be calculated by the following equation (*7*):

$$W_{ET} = \frac{A'_e}{A_e} = \frac{\int_{\epsilon_d}^{\epsilon_c} f_1(\epsilon)\, d\epsilon}{\int_{\epsilon_o}^{\epsilon_c} f(\epsilon)\, d\epsilon - \int_{\epsilon_d}^{\epsilon_c} f_1(\epsilon)\, d\epsilon} \qquad (1)$$

where $W_{ET}$ = energy index,
$A'_e$ = energy elastically accumulated in a sample,
$A_e$ = energy losses due to permanant strain,
$\epsilon_c$ = total strain,
$\epsilon_d$ = permanent nonelastic strain,
and $\epsilon_o$ = strain at zero load.

For Polish coals, a $W_{ET}$ greater than 5 meant the coal was liable to bump. This translates to a relationship where strong coal stores more strain energy and, as a result, is more liable to bumping.

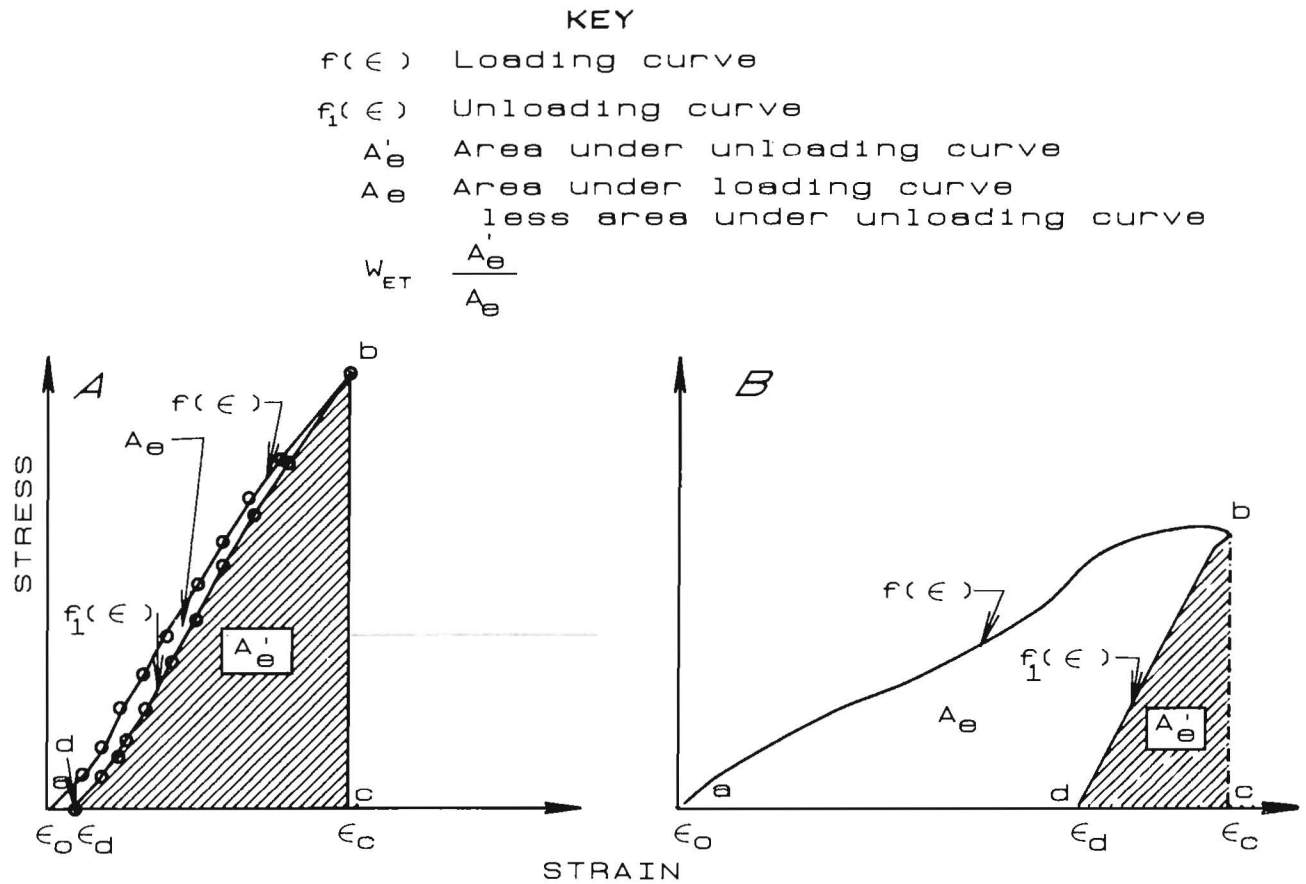


Figure 2.—Stress-strain curves for elastic and elasto-plastic coals (*7*) *A*, Bump prone, $W_{ET} > 5$; *B*, not bump prone, $W_{ET} < 2$.

Roof and floor rocks accumulate strain energy when stressed as plates or beams; beams release tremendous amounts of energy when failure occurs (*8*). The amount of elastic strain energy, $W_r$ for uniformly loaded cantilever and fixed-end beams is given by the following expressions (*9*):

$$W_r = \frac{Q^2\ell^5}{40EI}, \text{ cantilever beams,} \quad (2)$$

$$W_r = \frac{Q^2\ell^5}{1440EI}, \text{ fixed-end beams,} \quad (3)$$

where $W_r$ = elastic strain energy stored per unit volume,
$Q$ = load per unit length,
$\ell$ = length of beam or opening width,
$E$ = Young's modulus,
and $I$ = moment of inertia.

Strain energy is proportional to the fifth power of the beam length or opening width ($\ell$) for cantilever and fixed-end beams. Therefore, the length of beam in cave areas and opening width are critical factors influencing the occurrence of rock bursts or coal bumps in mines with strong roof and/or floor.

A large portion of the stored energy is released at failure. The amount of strain energy stored in the coal is also greatly dependent on the coal modulus of elasticity and can be determined using the following equation (*9*):

$$W_c = \frac{1}{2E_c}\left[P^2 + 2\left(\frac{P}{M-1}\right)^2 - \frac{2}{M}\left[\left(\frac{2P^2}{M-1}\right) + \left(\frac{P}{M-1}\right)^2\right]\right], \quad (4)$$

where $W_c$ = elastic strain energy stored per unit volume,
$E_c$ = Young's modulus of coal,
$P$ = principal stress,
and $M$ = coal Poisson's number (the inverse of Poisson's ratio).

Impact failures under lesser loads may occur because failure of strong roof can transmit an induced stress wave over a great distance, resulting in simultaneous bumps over a large area. This domino effect occurs when sudden loading causes high stresses to develop in a progressive manner (*10*).

## GEOLOGIC CHARACTERISTICS

The association between bumps and geologic conditions, e.g., fractures, joints, faults, and folds, has not been fully investigated. Past research indicates that rock burst frequency depends on mine location and the interaction between specific geologic features. Generally, thick overburden and steeply dipping seams are coincidental with bump conditions. Steep terrain, which causes rapid fluctuations in overburden pressure, and strong overlying strata, which may be resistant to rapid caving, are contributing factors to a bump. Although thick coal seams are more prone to bumping, the thickness of the coal seam alone is not a principal factor; thin coal seams have also experienced bumping depending on other contributing factors.

The location and orientation of geological anomalies, such as faults, folds, dikes, and joints, often contribute to bump conditions. The interaction of these anomalies and bumps is very difficult to determine, and opinions on the subject vary significantly. For example, substantial disagreement exists on the effect that faulted areas have on bump occurrence. In a study of Upper Bavarian seams in the Federal Republic of Germany, it was noted that bumps usually occurred in nonfaulted areas, while faulted areas had very few bumps (*11*). According to this study faults cause many microcracks to form, releasing excess stresses; the faulted area is less likely to bump. In addition, faults can absorb high amounts of strain energy and reduce the number of bumps. Contrary to these observations, substantial evidence indicates that bumps occur more frequently in and around fault zones. At the Spring Hill Mine in Canada, strong bumps occurred near fault areas during development of inclined headings (*12*). At the Sunnyside Mines, Sunnyside, Utah, the occurrence and magnitude of bumps increased considerably as the entries were developed through an 18-ft displaced fault zone. As a result, alternate means of support were needed to support the slopes (*13*). In Upper Silesia, Poland, the Andreas No. 3 Seam is folded by an overthrust fault along a 1,500-ft zone. Below the fault, explosive bumps occurred, while the area above the overthrust zone was free from bumps. The 360-ft depth cannot justify this abnormality. Scientists reasoned that stress was released above, but not below, the fault zone (*11*). In South African mines, bumps normally increase as mining faces approach a fault zone (*14*).

Experience indicates that greater stress levels will occur in dikes present in the seam mined (*11*). The increased temperature, metamorphism, and recrystallization of rocks near dikes may increase the spontaneous energy and uniformity of rock mass (*15*). Hackett (*14*) believes the presence of dikes will increase the incidence of bumps.

Experience also indicates that mining under synclinal folds may increase the frequency of bumps. Synclinal folds are normally jointed as a result of high lateral ground stresses. At the Knurow Colliery in Poland, crosscuts developed beneath small synclinal fold axes were difficult to maintain; however, as mining advanced through the synclinal region, crosscuts remained stable. At the Miechowice Colliery in Poland, mining under synclinal folds resulted in a large number of bumps (*11*).

Steeply dipping seams have also experienced bumps. A greater occurrence of bumps was found on the dip side of the seam at the Coal Creek Mine in Canada (*16*). Increased floor disturbances and hazardous bumps were observed in pillars near the low side of the entry (*17*).

The effect of overburden thickness on bump occurrences varies depending on the geological setting and mining method of the coal seams. Holland (*3*) indicated that overburden thickness exceeding 500 ft is necessary to cause bump conditions. While bumps were not reported in the Springhill No. 2 Mine, Nova Scotia (*18*), until mining reached a depth of approximately 1,900 ft, Rice (*19*) reported that bump occurrences were possible at depths exceeding only 1,000 ft in some mines in Virginia and Kentucky.

Existence of competent massive strata in close proximity to the coal seam is reported by numerous scientists to be a major contributor to bumps. Depending on the physical properties and thickness of the roof, strong sandstone roof may cave in large blocks caused by the bending stresses without any horizontal relaxation movements. If softer shale beds with smooth bedding planes are present, there will be a slow stress-relieving process of rolling out of the shale, which will allow horizontal movement of the coal toward the opening. This occurs because the coefficient of friction between shale and coal is low. The friction between coal and sandstone is often very high, which prevents horizontal relaxation of the coal. Coal is constrained by frictional forces induced by the sandstone with the abutment peak close to the opening. Coal located at an abutment peak will be confined and heavily

loaded. Sudden loss of friction between the coal and sandstone will result in a loss of much of the coal strength exhibited under a triaxial state of stress (confined). The coal will fail under excess loading and release the stored strain energy.

Soft shale beds, one to two times the thickness of the coal seam located between the seam and an overlying bed of massive strata, are usually sufficient to allow horizontal relaxation of the coal, thus preventing the formation of conditions that may result in bump.

Other geologic characteristics, such as the existence of strong floor rock that does not readily heave, stressed and steeply dipping seams, and mountain terrain, may also be contributors to bumps.

In general, the extent and degree of geological disturbance experienced in a coal deposit can create the necessary conditions for rock bursts or coal bumps. Major geologic intrusions, such as extensive folding in the coal seam, can cause high-stress anomalies to occur and increase the risks of a localized bump. Evidence suggests that a careful geologic study of the general mine area should be conducted prior to mine planning, for prevention of bumps.

## MINE DESIGN

Inadequate mine planning or incorrect mine design can increase the occurrence of bumps in underground coal mines. While many factors exist in the bump problem that cannot be controlled, mine design is one variable over which the mine operator has some control. A study (*9*) revealed that approximately 80 pct of the documented coal bumps occurred near pillar lines during retreat mining. A pillar-line point is a highly stressed area of a pillar that projects into the gob. Frequency of bumps in coal mines was categorized based on mining method and place of occurrence (fig. 3).

Bumps occur three times more frequently in room-and-pillar mining than in longwall mining (*9*). If a mine uses the room-and-pillar method and experiences bumps, then one possible solution would be for the mine operator to try longwall mining. This is, however, highly dependent on mining cost, geology, and reserves.

Multiple-seam mining can also contribute to bumps (*20*). Mining above or below other mine workings may cause an increase in the abutment pressures due to interaction between abutment zones. Multiple-seam mine planning should be scheduled so that abutment loading is not superimposed on active workings in adjacent seams. Remnant pillars left unmined in the seam being extracted, or in coal seams previously mined above or below the present operation, may also contribute to bumps (*9*).

During retreat mining, pillar recovery should be practiced in the destressed zone between the gob line and the abutment to reduce the potential for a bump. Since the abutment stress is typically on the first line of pillars, these pillars should be split prior to recovery. Pillar splitting causes yielding and load transfer onto the next line of pillars, creating a new abutment zone. This method of pillar recovery may be practiced in most bump-prone mines since strong roof strata normally exist. However, if the roof is weak, this method may cause roof control problems (*9*).

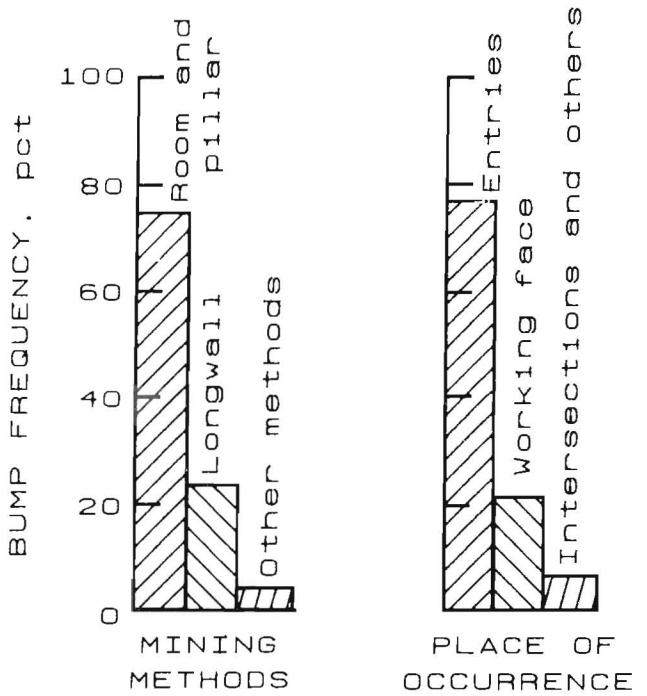


**Figure 3.—Bump frequency by mining method and place of occurrence.**

Strong and competent roof strata are a contributing factor to the bump problem and should be considered in the mine design. These strata often overhang behind the longwall face supports and in retreat room-and-pillar mining, creating excessive stress on the face due to a cantilever effect. If caving is inadequate, the abutment zone does not advance with mining; stress on the face may increase to a critical point and result in a bump. The critical point is reached when the stress in the abutment zone exceeds the ability of coal to store strain energy. This phenomenon is illustrated in figure 4.

## PHYSICAL PROPERTIES

Until recently, it was believed that brittle coal with a high compressive strength was a necessary element for bumping; however, Babcock (*21*) of the Bureau showed that coal composition was not the controlling factor, but rather the strength of the roof and floor. Strong roof and/or floor provide constraint to the pillar, and allow the pillar to build up large amounts of strain energy before failure. A weak roof and/or floor will allow the pillar to expand, deteriorate, and crush without a violent bump. Model coal pillars from 15 different coal seams in 6 States were tested; coal from 13 seams was made to bump regardless of the strength. These tests also revealed, contrary to previously published findings, that model pillars with a large width-to-height ratio (8.5:1) are not indestructible and can be made to fail or bump violently.

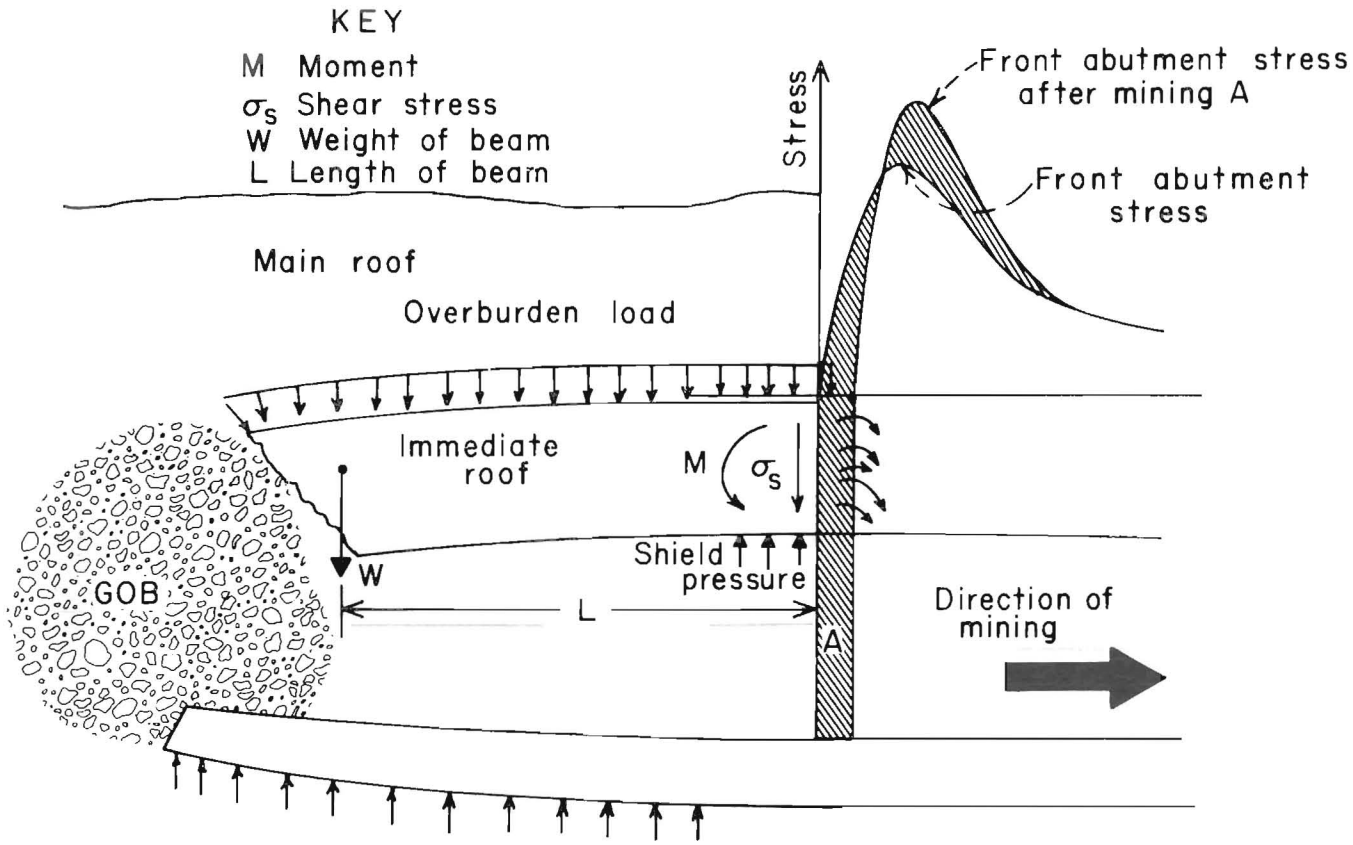


**Figure 4.—Front abutment stress profile caused by roof overhang behind face.**

## FIELD STUDY

A Bureau in-house research project was initiated to determine stress changes in pillars and longwall panels in a deep bump-prone western coal mine at various stages of mining. This study provided a unique opportunity to observe prebump and postbump behavior and the effectiveness of various techniques to control or prevent bumps in underground coal mines.

### MINE DESCRIPTION

The selected mine is located in western Colorado. It is operating at a depth of nearly 3,000 ft, with other active mine workings located about 400 ft above the coal seam being studied. The advancing longwall mining method is used to mine a 10-ft-thick coal seam dipping at 12°, with gate entries 16 ft wide. The long axis of the longwall panel is oriented parallel to the strike of the seam. The mine operates one main development section and one 800-ft-wide longwall panel. Upslope from the longwall panel are a previously mined longwall panel and pillared workings from old room-and-pillar sections. The general layout of the mine is shown in figure 5. Roof support in the entries is accomplished by mechanical anchor or resin-grouted roof bolts. Timber supports, trusses, and steel arches are also used in some areas of the mine.

### MINE GEOLOGY

The mine is in the Coal Basin Seam. The immediate roof, approximately 5 ft thick, is composed primarily of strong siltstone, shale, and sandstone layers. The immediate roof is overlain by a 9-ft competent sandstone layer that does not readily fracture and often forms cliffs where it outcrops at the surface. The mine floor consists of a strong shale-sandstone layer ranging in thickness from 4 to 12 ft in different areas of the mine, and a lower coalbed beneath the shale-sandstone floor consistently measures 8 to 10 ft thick. Figure 6 shows the geologic column at the test site. Two well-defined faults were mapped across the longwall panels approximately 2,500 ft ahead of the starting room of the advancing longwall face.

### BUMP OCCURRENCES

Owing to the thick overburden and strong roof and floor strata, bumps and outbursts have occurred in the mine in areas where coal was mined by room-and-pillar and longwall methods. Until 1983, stress relief had been practiced only to destress longwall panel corners and mining sections at depths greater than 2,000 ft.

Soon after operation began on the new longwall panel, face bumps occurred. Between January 1983 and July 1984, nine major bumps were recorded. The bumps shown in table 1 were either triggered by mining or were induced during stress relief.

On April 20, 1983, after 618 ft of longwall advance, a major bump occurred that affected the tailgate entries and the face. The bump resulted in a rapid floor heave that extended approximately 1,200 ft along the tailgate entry and 300 ft along the face. In addition, it disrupted ventilation, stopped production, and damaged 40 longwall shield supports. Figure 7 shows the floor heave in the tailgate and headgate entries after the bump. The floor heaved to within 1 ft of the roof in some areas, but no significant roof separation was measured.

**Table 1.—Summary of major events at test site**

| Event | Date | Type | Cause | Location (between shields) | Face advance, ft | Mining direction | |
|---|---|---|---|---|---|---|---|
| | | | | | | From | To |
| | | | BEFORE DESTRESSING | | | | |
| 1 | 1/13/83 | Coal bump at face. | Mining | 25–36 | 271 | HG | TG |
| 2 | 2/22/83 | ..do | ..do | 15–37 | 411 | HG | TG |
| 3 | 2/25/83 | ..do | ..do | 35–46 | 430 | TG | HG |
| 4 | 3/23/83 | ..do | ..do | 7–15 | 535 | HG | TG |
| 5 | 4/15/83 | ..do | ..do | 25–39 | 605 | HG | TG |
| 6 | 4/20/83 | Rock bump at floor | ..do | 125–162 and TG. | 618 | TG | HG |
| | | | AFTER DESTRESSING | | | | |
| 7 | 9/17/83 | Rock bump at floor | Volley firing | 150–162 and TG. | 1,000 | NAp | NAp |
| 8 | 1/28/84 | Rock and coal bump at floor and ribs. | Volley firing and water infusion. | 152–185 and TG. | 1,357 | NAp | NAp |
| 9 | 6/18/84 | Rock bump at floor | ..do | 125–162 and TG. | 1,877 | NAp | NAp |

HG Headgate. NAp Not applicable. TG Tailgate.

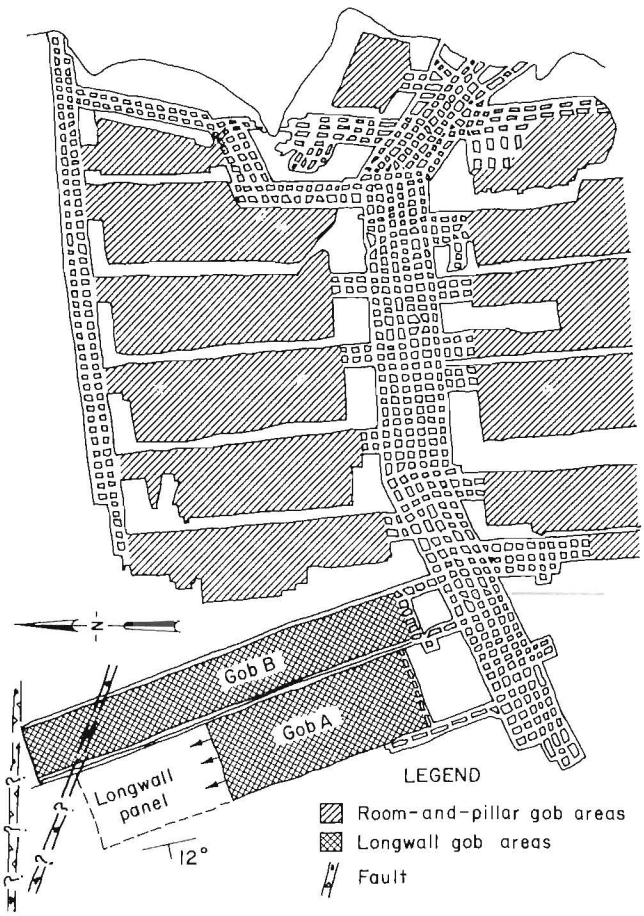


Figure 5.–General layout of study mine.

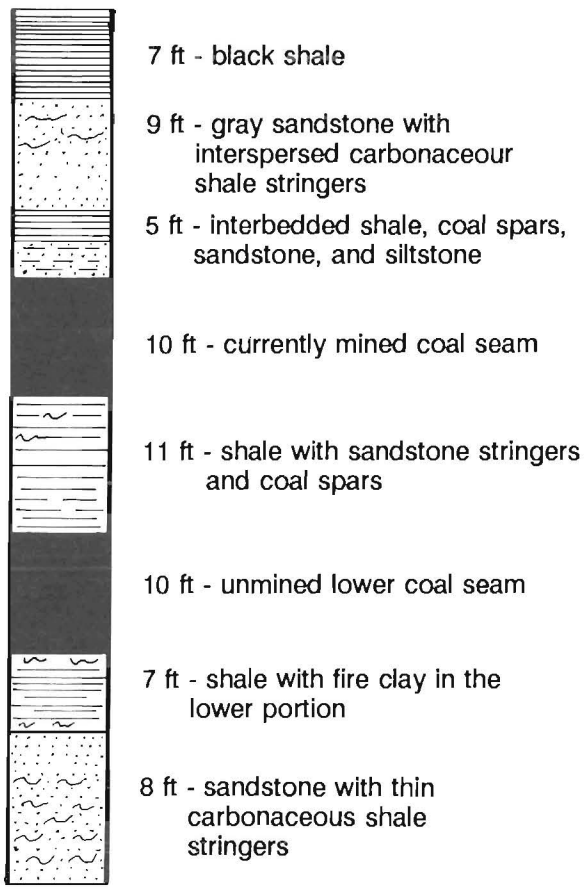


Figure 6.—Geologic column at test site.

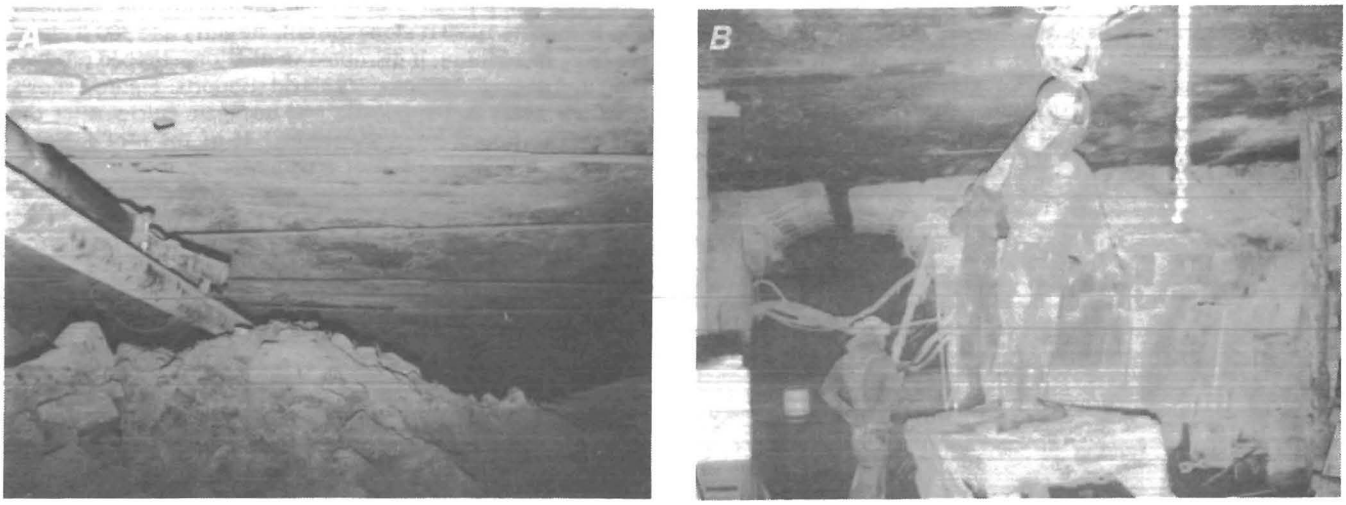


**Figure 7.—Headgate and tailgate entries after April 20, 1983 bump. *A*, Tailgate entry; *B*, headgate entry.**

After this bump, mine management incorporated a bump-control plan to safely continue production. The program consisted of detecting high-stress areas by using the drilling-yield method and by destressing such areas using volley firing. After the program was incorporated into the mining cycle, the longwall panel was mined to completion, advancing 3,900 ft, with essentially no uncontrolled bump occurrences. Nearly all face bumps were eliminated; those bumps that did occur were mostly in the tailgate entry and involved floor heave.

## SUPPORT SPECIFICATIONS

The longwall face is supported by 162 two-leg shields having 82.3-in$^2$ cylinder area per leg, 250 ton [3] per leg yield load, and 6,090 psi yield pressure. The maximum open height of each shield is 146 in, while the minimum open height is 70.8 in. The shields also have high-volume pressure relief valves to prevent shield leg damage during extreme bumps or floor heave. The maximum floor pressure is 345 psi.

# BUMP DETECTION METHODS

## BACKGROUND

Many attempts have been made to detect bump-prone (high-stress) areas ahead of mining. State-of-the-art equipment and technology have been used to the fullest extent. Detection of bump-prone areas involves locating high-stress zones in the coal seam or neighboring rock masses. Although several methods have been used, none is completely reliable, and few are useful in a rapidly advancing mining environment. The following high-stress detection methods are discussed: microgravity, rheological, rebound, photoelastic, on-site detection device, convergence, drilling-yield, and microseismic. Detailed discussion of the drilling-yield and the microseismic methods utilized at the study mine is presented in the section "Detection methods used at test site".

### *Microgravity method (22)*

The microgravity method uses rock mass deformations, changes in gravity intensity, and change in density distribution to evaluate bump-prone areas. Stresses in rock mass disturbed by underground mining will redistribute and reach a new equilibrium. The resulting density distribution is a function of a change in rock mass volumetric strain. Strain energy released in the form of a bump is approximately equal to the change in gravity intensity.

Changes in density distribution occur with postmining rock mass deformations, produce measurable changes in gravity microanomalies, and appear in four stages of brittle fracture of rocks in multiaxial compression: crack closure, fracture initiation, critical energy, and maximum deformation (rupture).

Rock bumps may be predicted depending on the gravity anomaly sign recorded; a negative gravity anomaly occurs shortly before a bump, while a positive gravity anomaly indicates a bump is not likely to occur. A negative gravity anomaly is caused by an increase in volume and a decrease in rock density.

### *Rheological method (23)*

The rheological method incorporates the rate of stress relaxation and the level of coal disintegration to predict coal bumps. Stress relaxation rates depend on mechanical properties of the coal, geological conditions, seam depth, rate of advance, and stress concentration in the coal. A low relaxation rate, combined with a high disintegration rate, indicates the coal is bump prone.

### *Rebound method (23)*

The rebound method can be used to predict bumping tendency of the coal seam from resilience tests conducted in situ or on core samples. The assumption is that the energy released during bumping is proportional to the strain energy stored within a unit volume of coal. The results are expressed

[3] In this report, "ton" indicates 2,000 lbf.

as an energy index, $W_{ET}$. The test uses the Schmidt hammer with a single impact energy of 0.75 J. The energy index can be obtained using the following equation:

$$W_{ET} = e^{(0.06R^2 - 1.76)} \quad (5)$$

where $W_{ET}$ = energy index,
R = Schmidt rebound index,
and e = mathematical constant of value = 2.718.

Based on practical experience with the application of this criterion with respect to bump-prone coal seams, coal was classified as follows:

a. If $W < 2$, coal is not likely to bump.
b. If $2 < W < 5$, coal is likely to bump.
c. If $W > 5$, coal will probably bump.

*Photoelastic method (24)*

When certain plastics and optical glasses are subjected to stress and viewed under polarized light, the patterns of interference become visible and can be related to applied stress intensity and direction.

1. The disk technique is fairly inexpensive and does not require extensive expertise. Plastic material is bonded to the rock under load and placed on the surface of an existing excavation or at the flattened end of a borehole. The disk technique is best suited for igneous rocks with good elastic properties under high stress.

2. The prestressed meter technique uses a device, containing an appropriate glass plug, placed inside a borehole and prestressed against two opposite points on the hole wall by jacking platens operating through wedges. The stress magnitude is given in terms of an interference fringe pattern, which can be seen under polarized light. The fringe pattern is measured with a special mechanism calibrated in fringe units and gives stress magnitudes. The prestressed meter technique is limited by the depth of the borehole because of viewing limitations.

*On-Site Detection Device Method (25)*

The on-site bump detection device can be attached to an underground mine surface and provides a signal of the stress concentrations in the surrounding coal or rock to indicate if a bump may occur. This is based on the principle that rock under stress produces a current varying greatly with rock type. Current is recorded for a 24-h period, and the detector automatically resets if the stresses remain below a certain point.

*Convergence Measurements Method (26)*

This method is widely used because it is easy and inexpensive. Convergence or convergence rates are monitored either at the face during mining or in the entries. The method is mainly used if the mine experiences shock bumps in the roof.

## DETECTION METHODS USED AT TEST SITE

### Drilling-Yield Method

The drilling-yield method, also known as the probe-hole drilling method, has been used in the U.S.S.R. since the 1950's. In the early 1960's, the method was modified and adapted to local and geological conditions in a few of the European coalfields. Recently, the method was introduced to the U.S. mines and was favorably accepted at the test site. This in-mine method, very simply, involves drilling holes into the coal panel or pillar, usually with an auger drill, and recording the volume of drill cuttings obtained from a given hole depth. A certain volume of cuttings can be expected from a drill hole that has a known diameter and length. If the actual volume of cuttings generated exceeds the volume of the hole by a significant amount, the zone around that particular hole is determined to be highly stressed. Drilling in a previously stressed zone produces compression in the borehole. Various dynamic effects are observed, such as audible knocking (bumping) and jamming of the drilling rod in the borehole. The closer to the pillar edge a highly stressed zone is encountered, the greater the danger of rock bumping. Typical curves obtained from drilling in a 7-ft-high coal seam, showing the drilling results for a dangerous (high-stress) and nondangerous (low-stress) zone, are presented in figure 8.

Based on past studies (*7*), the bump potential is determined from the drilling-yield results and mining height or seam thickness (T). Usually, in most coal mines, the mining height equals the seam thickness. These relationships are summarized as follows:

- If the increased stress zone is detected at a distance greater than 3.5 times the mining height (T) measured from the rib side, a safe mining state is assumed. Mining can progress, and no destressing is required.
- If the increased stress zone is detected at a distance between 1.5T and 3.5T from the rib side, a dangerous mining state exists. Mining may or may not progress, depending on many other factors, such as physical properties, geologic conditions, and the amount of stress increase in the zone.
- If the increased stress zone is detected at a distance less than 1.5 T from the rib side, a critical bumping condition exists. Mining should stop, and destressing should be practiced.

Since geologic conditions and rock physical properties vary in different mines, these results may need further confirmation before application to a specific mine.

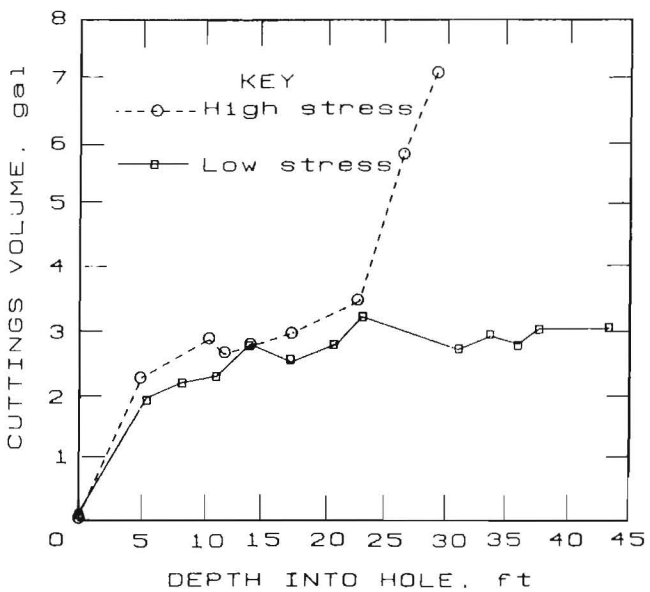


**Figure 8.—Drilling-yield results.**

## Theory

The idea of probe-hole drilling is based on the theory of stress around a circular opening. The magnitude and distribution of the stresses around a single underground opening in massive rock, such as a drill hole in a thick coal seam, have been determined analytically and from laboratory model studies (*27*). The stress concentrations around a circular opening in a bidirectional stress field are shown in figure 9. This figure shows that for a material with Poisson's ratio of 0.25, the boundary stress concentration around the circular opening can be obtained. When the boundary stress exceeds the strength of the material, the hole begins to deform and possibly fail. When the applied stress is high, as is the case with the forward abutments ahead of a longwall face, it is easy to see why the hole fails as it is being drilled. For highly stressed areas, the coal around the drill hole behaves plastically and flows into the hole.

## Field Procedure and Results

At the study mine, the drilling-yield method was used to locate high-stress zones in the longwall face. Probe-hole drilling was conducted using a handheld air-powered auger drill with auger rods 3 to 5 ft long. Along with the auger rods, a two-wing, 2-in-diam, carbide-insert drag bit was used. Technical information and drill specifications for the drill used are listed in the appendix. Drilling operations consist of a two-person crew, a driller and a helper who assists in adding auger rods and recording the following information: volume of cutting produced per length of hole drilled, occurrence of bounces, location of gas in the hole, and squeezing of the hole on the drill rod. A typical drilling-yield field data form is shown in figure 10. Site preparation involves scaling the rib or face to provide a solid, stable surface for the collar of the hole. Actual drilling involves controlling penetration rate to prevent sticking the auger steel in the hole. Because the drill is handheld, the driller's experiences are critical to locating the high-stress zone. Drilling was always performed while the longwall face was not operating.

The area is determined to be highly stressed if the volume of cuttings from the 2-in-diam hole exceeds 5 gal per 3-ft length of hole drilled, or if the driller hears or feels minor bouncing or constant hole squeezing, and auger steel jamming is recorded during the drilling. The presence of large volumes of gas blowing from the hole is also used as an indicator of high-stress zones.

The drill pattern at the test site consisted of drilling 2-in-diam probe holes on 50- to 100-ft centers along the length of the longwall face on a daily basis. The results are plotted to show the areas of high stress ahead of the face. Figure 11 shows typical drilling-yield data from three drill holes. In hole 1, for example, more than one abutment zone exists within the length of the hole at this location. The abutment zone in hole 1, which fits the criteria for critical stress, occurs at a depth of approximately 49 ft ahead of the face. At this mine, if drilling-yield results show an abutment zone existing at a distance away from the face greater than at least three times the seam height, the face is generally determined non-bump-prone, and no destressing is performed.

## Laboratory Tests and Results

Probe-hole drilling, as proven by in-mine experiences, can give reliable information on the general stress state in the coal seam. The absolute stress magnitude is not determined, however. Laboratory tests were performed to find a relationship between stress magnitude and volume of cuttings. The tests were conducted using 4-in simulated coal (coalcrete) cubes that were compressed using a developed test frame (fig. 12). Coalcrete is a mixture of 47 pct coal, 37 pct fly ash, 7 pct cement, and 9 pct water. The average compressive strength of the coalcrete is 1,500 psi, and Young's modulus is $3.0 \times 10^5$ psi. Tests were conducted under different confining pressures. The results (fig. 13) show the following linear relationship between the applied vertical stress and the log of $V_c/V_e$.

$$\text{Stress} = 17{,}800\ (\log V_c/V_e) + 2{,}670\ \text{psi}, \qquad (6)$$

where $V_c$ is the actual volume of cuttings obtained and $V_e$ is the volume of cuttings expected from the hole drilled. Results indicate that drilling yield may be used to indicate the general stress level in the mine.

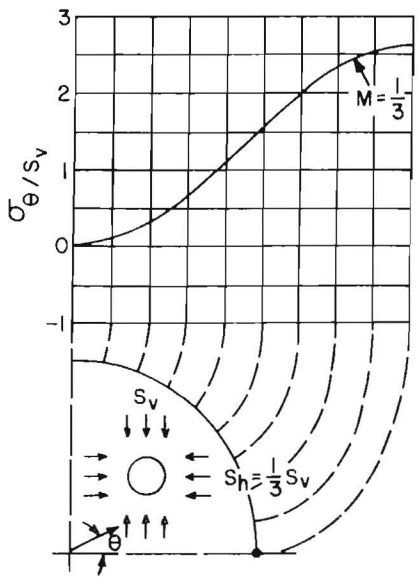


KEY

M Ratio of $S_h/S_v$

$S_v$ Vertical stress

$S_h$ Horizontal stress

$\sigma_\theta$ Stress at angle $\theta$

**Figure 9.—Boundary stress concentration for circular opening.**

Date: _____ Shift: Driller: _____

Hole diameter: _____ Hole location: _____

_____

DRILLING RECORD

Drilling start: _____ h

Drilling end: _____ h

\+ Low noise

○ Noise can be heard 60 ft away

● Noise can be heard 300 ft away

| Depth, ft | 3 | 6 | 9 | 12 | 15 | 18 | 21 | 24 | 27 | 30 |
|---|---|---|---|---|---|---|---|---|---|---|
| Volume of cuttings, gal | | | | | | | | | | |
| + | | | | | | | | | | |
| ○ | | | | | | | | | | |
| ● | | | | | | | | | | |
| Remarks | | | | | | | | | | |
| Depth, ft | 33 | 36 | 39 | 42 | 45 | 48 | 51 | 54 | 57 | 60 |
| Volume of cuttings, gal | | | | | | | | | | |
| + | | | | | | | | | | |
| ○ | | | | | | | | | | |
| ● | | | | | | | | | | |
| Remarks | | | | | | | | | | |

REMARKS, CODES

B Gas is blowing out of hole

F Drill cuttings are fine

G Drill cuttings are coarse

K Coal pressure squeezes drill

W Drill cuttings are damp

Z Drill is drawn into the coal

ST Rock is ahead

WW Drill cuttings are wet

**Figure 10.—Drilling-yield field data form.**

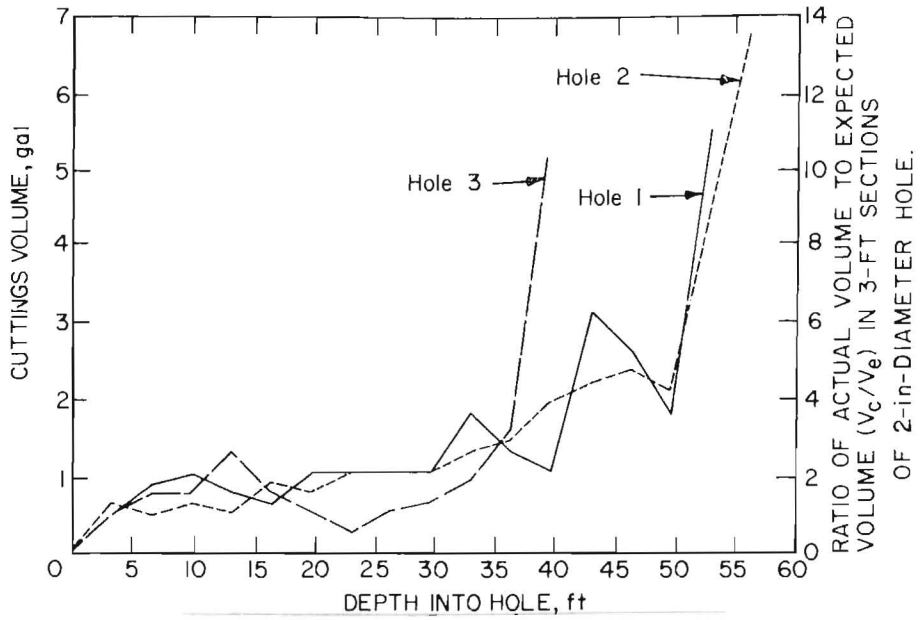


**Figure 11.—Drilling-yield data from three drill holes.**

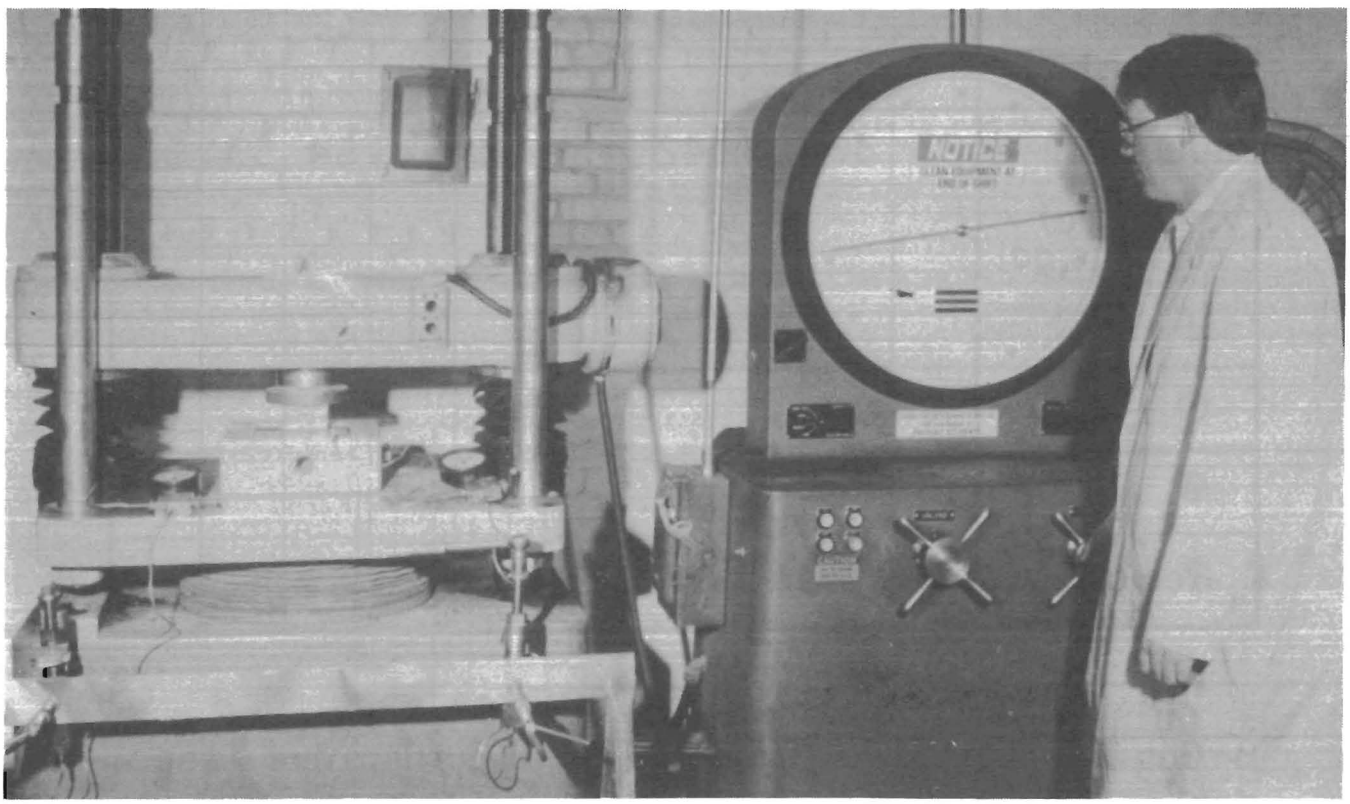

**Figure 12.—Arrangement of laboratory equipment for drilling-yield tests.**

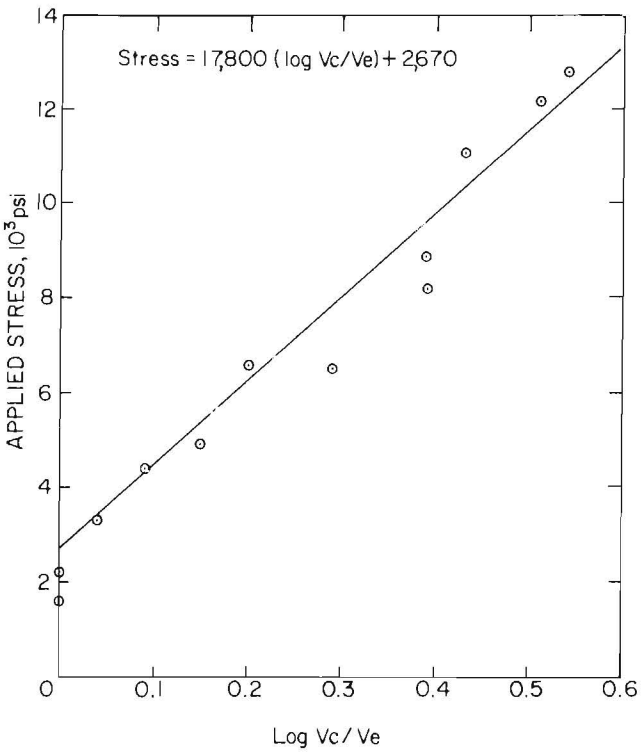


**Figure 13.—Laboratory test results from drilling-yield method.**

## Microseismic Method

The microseismic method, also known as the subaudible sounding or acoustic emissions (AE) method, is a geophysical approach that detects subaudible rock noise (microseisms) associated with yielding or fracturing of the rock. The useful frequency spectrum of rock noise detected by the system during longwall mining ranges from 160 to 500 Hz. Geophones translate the rock noises from acoustic waves, which may be undetectable by the unaided ear, to electrical analog signals.

In the late 1930's, Obert and Duvall (*17*) discovered naturally occurring rock noise while measuring seismic velocities in mine pillars. In 1941, they documented a dramatic change in rock noise rates prior to major failures in lead-zinc mines in Oklahoma and copper mines in Michigan. In 1945, they applied this geophysical technique to predict rock bursts by monitoring and listening to rock noise activities in bump-prone areas (*17*).

### Theory

Stress redistribution in coal and rock results from fracturing induced by either geological or mining stresses (*28*). Generally, the development of a rock fracture occurs in three stages: crack initiation, crack propagation, and ultimate fracture, each generating microseismic energy pulses (waves) whose magnitudes are proportional to crack size and displacement (*29*). The microseismic method is used to detect high-stress zones and potentially unstable areas and is based on experimental evidence that rock under load undergoes small-scale displacements, which result in the release of seismic and sometimes acoustic energy (*27–28*).

Laboratory testing of rock indicates increased noise rate with increased stress, the rate increase becoming pronounced as the ultimate stress is approached. Noise-rate curves prior to failure in different geological materials often exhibit similar slopes even though the materials and failure mechanisms are different (*30*). A pattern of increased activity followed by a very low activity period immediately prior to bumps in underground mines has been noted by several researchers, but this behavior has not been reproduced in the laboratory (*29, 31*). While some bumps are preceded by rapid increases in the microseismic noise rate, others show no rate increase, and sometimes, while rapid rate increases are measured, no bumps occur (*28, 32*).

Coal exhibits a very broad AE frequency spectrum that ranges from 100 Hz to 1 MHz (*29*). However, the most common frequency detected from laboratory testing of coal is 5 kHz (*31*). Both p compressional (*p*) and s shear (*s*) waves are present in the microseismic wave, but most of the energy is in the S-wave. Attenuation of the wave amplitude with distance depends on the frequency; low-frequency waves travel further, whereas high-frequency components of the wave form are rapidly attenuated with distance and increased travel time.

A good coupling between the geophone and the rock is required for good response to S-wave arrivals. Energy calculations from field data generally require the entire wave form (P and S waves), an average particle velocity determined from seismic velocity surveys, event duration, and average wave frequency from the seismic record, rock mass density, and accurate geophone-to-source distance (r).

### Source Location and Seismic Velocities

Qualitative analysis of microseismic data requires the accurate determination of each rock-noise source location. Several methods are available to calculate noise source locations provided that accurate geophone locations, seismic velocities, and arrival times are known. For the data analysis at the test site, the generated block with comparison method (GBLCK) was mainly used. Difficulties due to geology and anisotropy result in nonuniform wave fronts around each source. As seismic velocities may vary considerably with direction, it is important that source-to-geophone seismic velocity surveys be performed to accurately determine source locations and velocities (*28*). On-site velocity surveys are further complicated because of limited access to the rock mass and possibly because of opening access-stability for installing the geophone arrays. In other words, some areas of the mine are not accessible because of bad ground conditions.

The simplest method of velocity survey is to detonate an explosive at known coordinates and record both the shot times and arrival times at each geophone. Knowing the blast and geophone coordinates and the arrival times at each geophone, the in situ seismic velocities for both P- and S-waves ($V_{pi}$ and $V_{si}$) for each geophone are determined. Periodic seismic surveys of the mine should be conducted.

## Instrumentation

A microseismic system (fig. 14) consists of geophones to detect the rock-noise vibrations and convert them to electric signals, an amplifier to increase the level of the signal, and a monitoring-recording system to record the arriving signals. A computerization system assists not only in gathering data, but in processing and analyzing the signals and displaying the results. The frequency, amplitude, and pulse durations of anticipated rock noise must be considered in the selection of the proper geophones and amplifiers, so that the sensitivity of the array is optimized for maximum data acquisition.

Waves induce motion within the rock mass; the motion is described by displacement, velocity, and acceleration. Various types of geophones are available to record mass movements. Displacement gauges are most sensitive to low-frequency vibrations, velocity gauges for low- to moderate-frequency vibrations, and accelerometers for moderate- to high-frequency vibrations. As the rock-noise frequency spectrum is very broad, velocity or acceleration geophones are mostly used. Gauge-type selection depends on the characteristic frequency of the rock and on site-specific preliminary surveys: velocity gauges are used for soft rock and low stress, and accelerometers are used for hard rock and high-stress areas. At the test site, the velocity-type gauges were used.

Geophone positioning should provide good rock-noise source location and protection from hazards. Source location is very sensitive to the geophone array geometry. Ideally, a three-dimensional array that surrounds the study area is recommended for more accurate event locations. Geophones should be securely bonded to an intact, smooth rock surface to provide good response to the wave arrivals. If the rock surface is loose, plastic blocks should be attached to the rock surface before the geophones are installed.

Seismic events result in low output voltages that require amplification to drive the recording-monitoring system. Preamplifiers may also be needed when the signal is transmitted long distances via cable. The function of the preamplifier is to boost the signal for good signal-to-noise ratio. An amplifier is used to further boost the signal, which allows transmission over a long distance with minimal loss of signal strength to drive the recording equipment. The cable should be waterproof and have a high tensile strength to resist stretching or breaking. A four-conductor-shielded cable was used at the study mine and hung from the mine roof with insulated hangers.

Data analysis requires data recording and monitoring. Chart, strip, and oscilloscope recorders provide a visual record of noise occurrence, number of events, number of geophones detecting the event, and relative magnitudes. From multichannel, high-speed magnetic tape, the magnitude of the events and the time at which they occurred can be determined. Relative arrival times to determine event location and magnitude, as well as rock-noise and energy-release rates for any part of the mine structure and for three-dimensional mapping of increasing stress areas, can also be determined.

The seismic energy released from an event occurring within the perimeter of the array will travel outward from the source, and it can be picked up by the various geophones. The event arrives at different geophones at different times. The velocity of the seismic energy and the arrival times to each geophone provide the basis for calculating the coordinates of each rock-noise event. Each event is then plotted on the mine map to locate areas of seismic activity. Depending on the location of the events and the time span in which they occur, areas that are undergoing significant structural change may be detected.

## Data Analysis

Currently, application of the microseismic technique in coal mines is limited to the accuracy of individual source

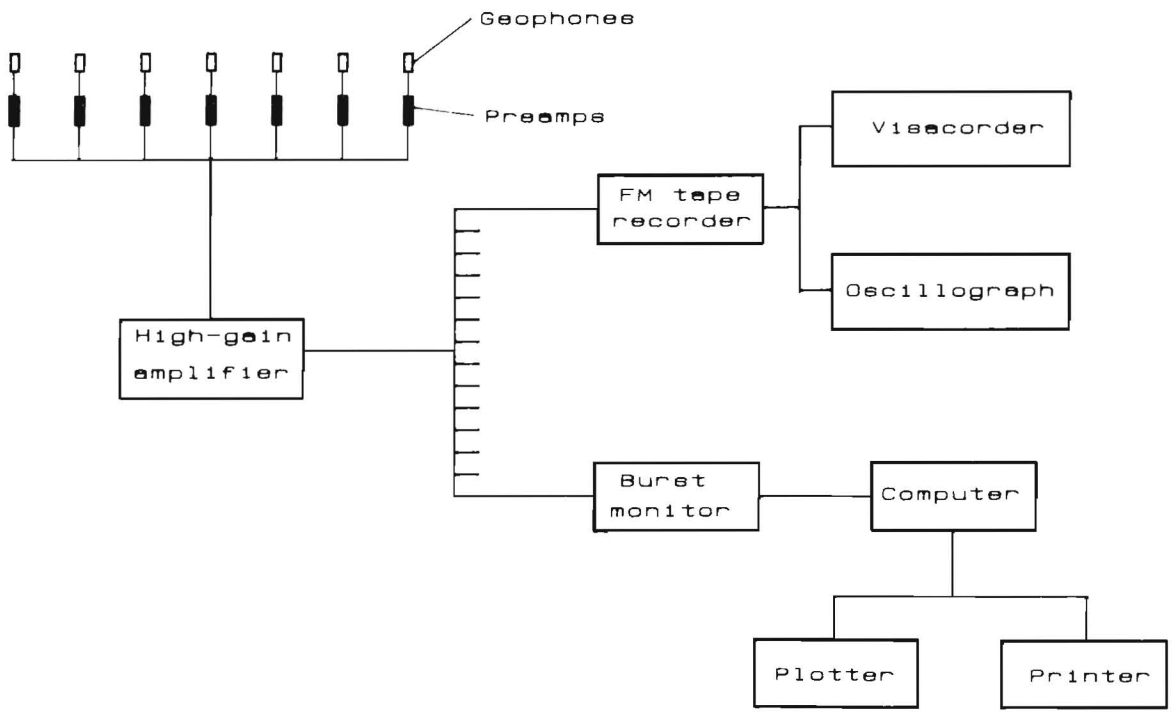


**Figure 14.—Schematic of microseismic equipment.**

locations and the development of a real-time analysis system. Source location limitations are dependent on site-specific conditions and often limited access to certain areas in the mine that prevents accurate, in situ seismic velocity determinations and/or complete coverage of the study areas. Since the advancing longwall mining system was used at the test site, geophone installation inby the headgate entry was prevented.

Microseismic data are generally used to identify high or increasing stress, or incipient movement within the strata, and to locate yielding or nonyielding zones. While audible rock noise often provides warning of the imminent danger, there is often a long period of subaudible noise generated in rock under stress. The fact that microseisms are generated in rock under stress, and that noise rate increases as failure approaches, provides the basis for detecting and delineating potential danger areas.

The microseismic method does not consider the stress state, rock mass strength, or any failure criterion other than the magnitude of the microseismic event rate. In the laboratory the noise rate varies with mineral composition, crystal size and bonding, and other factors. On the megascopic scale, joints, fractures, and other geological defects affect rock noise generation (*27, 29*). The method is not quantitative and requires experience to interpret; however, interpretation is facilitated by the fact that the near-failure noise rate may be 10 to 100 times the stable noise rate. Rock-noise rate versus time can be plotted with respect to specified time intervals; change in noise rate indicates instability. Although rock-noise counts are useful, correct interpretation of the data is difficult unless the data refer to specific portions of the mine structure. Meaningful interpretation may be possible (*30*) by using only locatable events relevant to the subject structure that are large enough to be detected on a few geophones.

While prediction is not the goal of microseismic analysis, it may be used to evaluate the stability of a structure. Structural stability analysis is based on the rock-noise count, energy-release rate, source location, and seismic velocity data. Complete analysis requires knowledge of the structure loading and the mining-induced load transfer. Structural loading in conjunction with the microseismic data may indicate how the mine structure is reacting and if failure is expected (*30*).

## Results

At the study mine, results of documented microseismic activity were analyzed against known bump occurrences. Acoustic emission locations were plotted on mine plan view drawings, and the acoustic emissions were compared to the bump occurrences. Figure 15 shows a plot of the acoustic emission events before the April 20, 1983 bump.

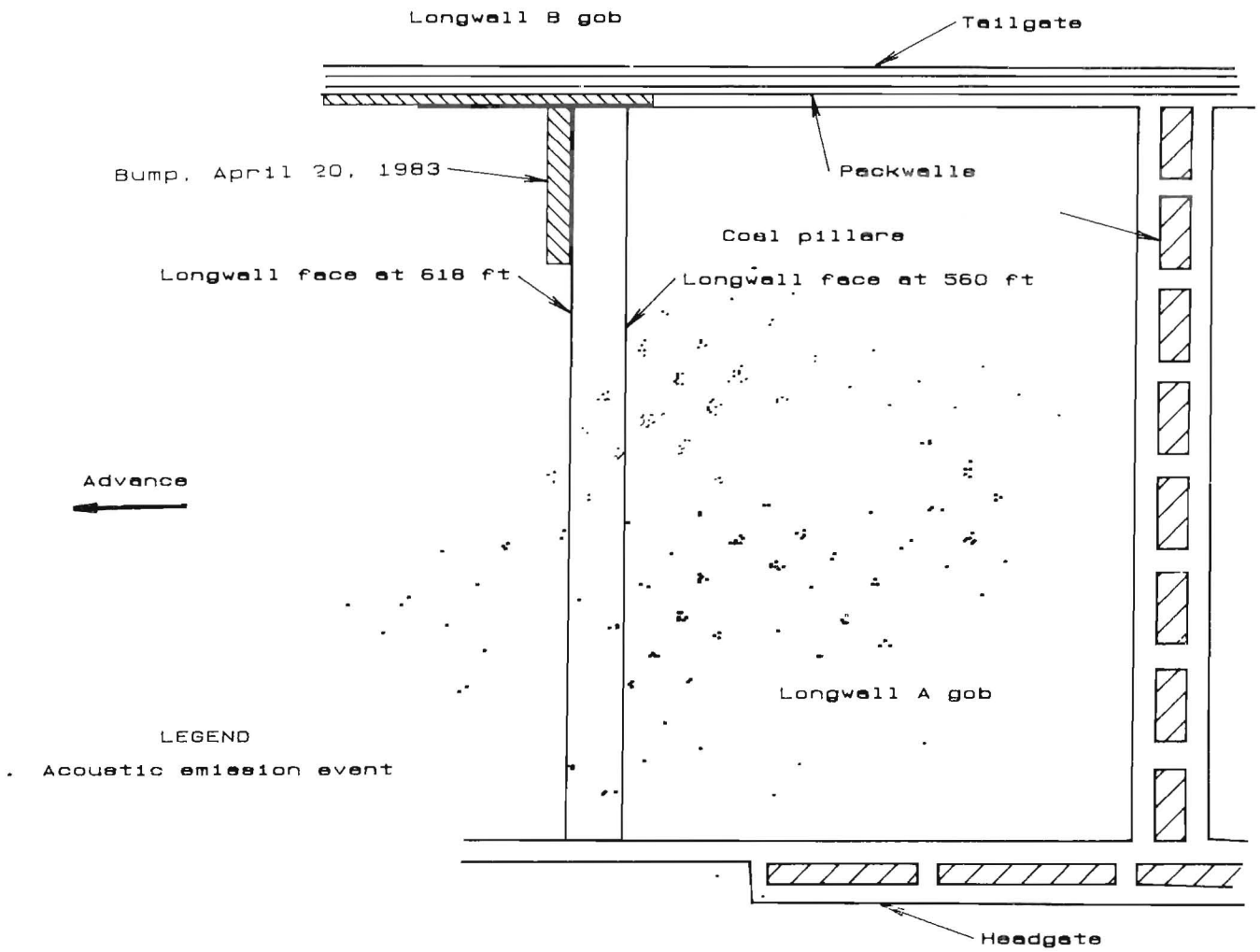


**Figure 15.—Typical acoustic emission event plot.**

In general, bump occurrences were located in areas that experienced a decrease in documented microseismic activity prior to the bump. This agrees with some studies that have observed decreased acoustic emission activity prior to bumps owing to fracture closure and coal seam microstructure.

The low-microseismic-activity zones were not a direct indicator of an impending bump. Even though the major bumps did occur in nonactive zones, not all nonactive zones experienced bumps.

Many questions still exist regarding the use of acoustic emissions in bump detection. Why do some bumps occur in nonactive zones while others do not? Interpretation of the acoustic emission data is highly dependent on individual observers and site-specific conditions.

# BUMP PREVENTION METHODS

## BACKGROUND

High stress is the common denominator in the bump problem. Causes of high stress can be traced to a number of factors, such as pillar size and shape, roof and floor confinement, coal material properties, mining method, rate of advance, cutting depth, and orientation of panel with respect to in situ stress fields. The contributing factors are numerous and present very complicated problems in predicting potential bump locations. Prevention of bump occurrence may be achieved by proper planning and mine design, sometimes including an active stress-relief program incorporated into the mining cycle.

Bump occurrences can be reduced in multiple-seam mining by superimposing the main entries and barrier pillars (*11*). This eliminates the need to cross the abutment zone of the adjacent seam. Also, mining should be scheduled between the seams so that abutment loading is not superimposed on the active workings in adjacent seams. When retreat room-and-pillar mining is practiced above or below other workings, full extraction is essential; leaving large pillar stumps should be avoided to reduce the potential of a bump. In longwall mining, yielding chain pillars shed their load as mining advances and are less likely to bump than are rigid pillars, which tend to store energy and bump violently.

In either advance or retreat mining, a means of controlling bumps involves mining between the abutment zones. When developing entries, the sequence of advancing should be designed so the abutment zone remains ahead of mining. The multiple-entry mining sequence shown in figure 16 was the most effective system used at the test site (*33*). Advancing entry 1 created an abutment zone represented by the stress profile shown in the figure. When entries 2 through 4 were advanced to the same distance in sequence, the abutment zones also advanced, and mining of the crosscuts was accomplished safely. This process was repeated after all the crosscuts were mined.

## DESTRESSING METHODS

The basic concept of destressing or transferring high-stress concentrations from one portion of a mine structure to another is not new. Fracturing or softening rock or coal to control stress buildup has been practiced in various mines. In coal mines, destressing the active working face is the most logical method to prevent bumps.

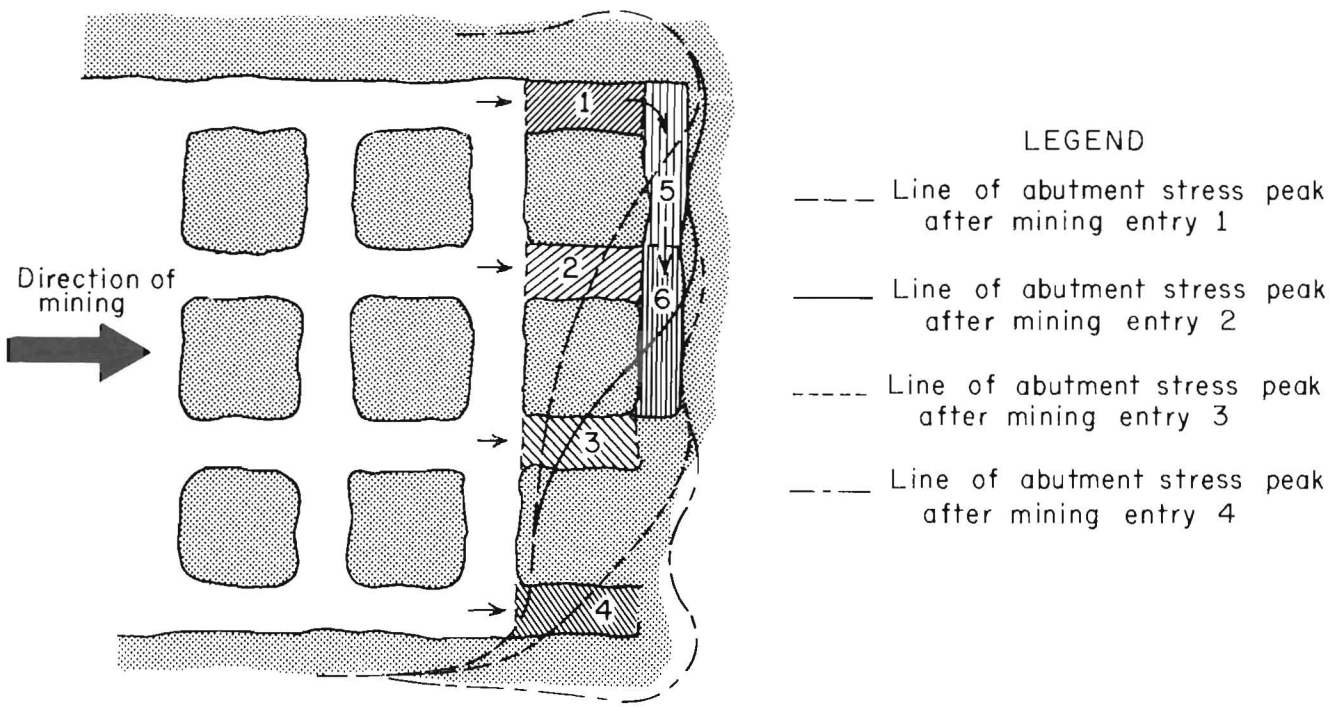


**Figure 16.—Effective mining sequence for advancing development section in bump-prone mine.**

Although different destressing methods have been used, all methods are based on the same theory. Coal, or in some instances roof and/or floor rock, is intentionally fractured and made to fail. As a result, no high-stress buildup can occur in the fractured zone, and the load is transferred to another part of the mine structure. If stress cannot build up, the area will not bump violently. The theory is simple, but controlling the extent of the fracture and the rate of load transfer is not always feasible. Occasionally, destressing itself may trigger a bump, but mine personnel are usually remote from the working face during the stress-relief operations. For example, in volley firing, workers drill only small-diameter holes and then retreat to a safe distance while the holes are fired to destress the area. Overall, worker safety is increased by a stress-relief program.

Three major destressing methods used in coal mines are discussed in the following sections. The effectiveness of these methods is largely dependent on mine conditions.

## Volley Firing

Destressing by volley firing has successfully reduced the number of rock and coal bumps in underground mines (*34*). In the volley firing method, explosives are used to fracture the coal face to a certain depth before mining. The method is used prior to face advance or entry development to advance the abutment zone away from the active working face.

Longwall face stress relief is accomplished by drilling into previously located high-stress zones (fig. 17). The blast holes are loaded with 3 lb of permissible explosives, stemmed, and detonated. The drill pattern consists of a series of 2-in-diam holes, 13 to 15 ft deep, drilled on approximately 4-ft centers. Hole depth depends on the required daily advance of the face and on the location and magnitude of the stress abutment ahead of the face. Local conditions and site-specific experience dictate exact hole parameters. The corners of the advancing longwall face require a radial drilling pattern, using combinations of two or three holes angled at 10° and 45° (fig. 17) to relieve high stress in both the face and rib areas.

Destressing a longwall development section or room-and-pillar entry working face may also be required. Figure 18 illustrates a volley-fire, drill-hole pattern for a development section. Holes are angled into the rib in a pattern similar to that for the corners of the longwall face. The drill holes do not extend deeply into the rib because blasting the rib effectively reduces the load-carrying area of the pillar. The depth and angle of the rib holes thus depend on the size of the pillar, the distance of the abutment zone from the face and entry, and other local conditions.

## Hydraulic Fracturing

This method involves the injection of fluid under pressure to overcome compressive stresses and to cause material failure by creating fractures or fracture systems in a porous medium. Hydraulic fracturing is most effective in the roof and coal seam ahead of the longwall face. This method is time consuming and not recommended for use on the face because it interferes with production.

Experiments conducted in Poland (*35*) have shown the beneficial effects of hydraulic fracturing of the roof ahead of the longwall face. Significant decreases in the number of seismic events during mining occurred in zones where the roof had been hydraulically fractured as compared with zones that had not been prefractured. During fluid infusion, the number of seismic events increased, an indication that the fracturing process probably caused stress redistribution.

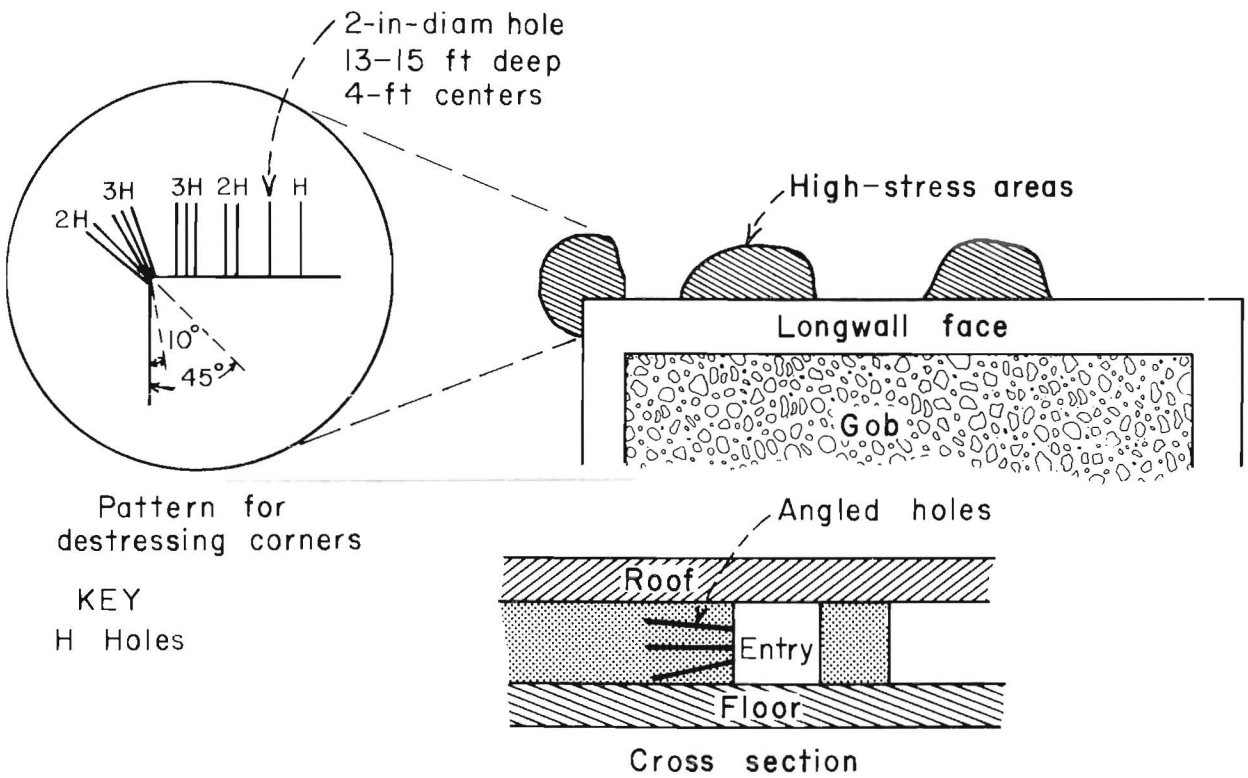


**Figure 17.—Volley firing drill-hole pattern for longwall faces and corners.**

Hydraulic fracturing of the coal seam ahead of the face is also practiced. Figure 19 shows a sample drill-hole pattern into the rib of an advancing longwall panel. Fluid under high pressure is injected into the holes. The pressure needed for fracturing is dependent on the physical properties and in situ stresses for coal and adjacent strata. At the study site, the fluid pressure was calculated using the following equation:

$$F = (1 - \nu)(x + \tau), \quad (7)$$

where $F$ = fluid pressure,
$\nu$ = Poisson's ratio,
$x$ = horizontal rock bed strength,
and $\tau$ = tensile strength.

Numerous variables affect hydraulic fracturing, including prevailing rock stress, rock tensile strength, modulus of elasticity and Poisson's ratio of the rock, rate of fluid injection, injection time, fracture clearance, formation permeability and porosity, fracture fluid viscosity and pressure, and total fluid volume injected. Controlling the extent of the fracture zone is very difficult because of the many variables associated with

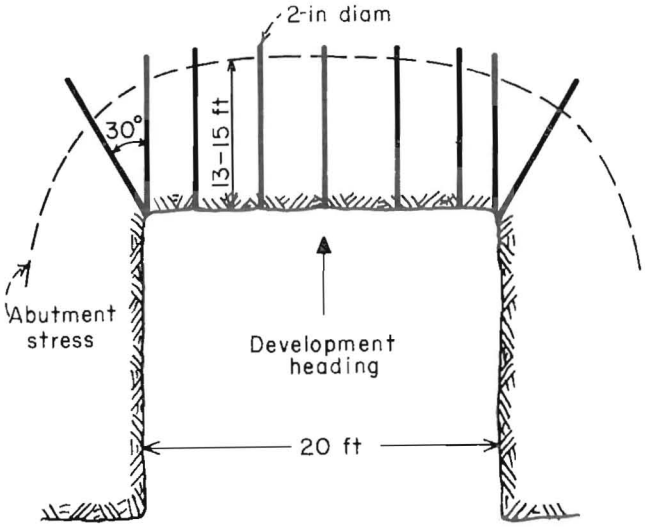


**Figure 18.—Volley firing drill-hole pattern for development entries.**

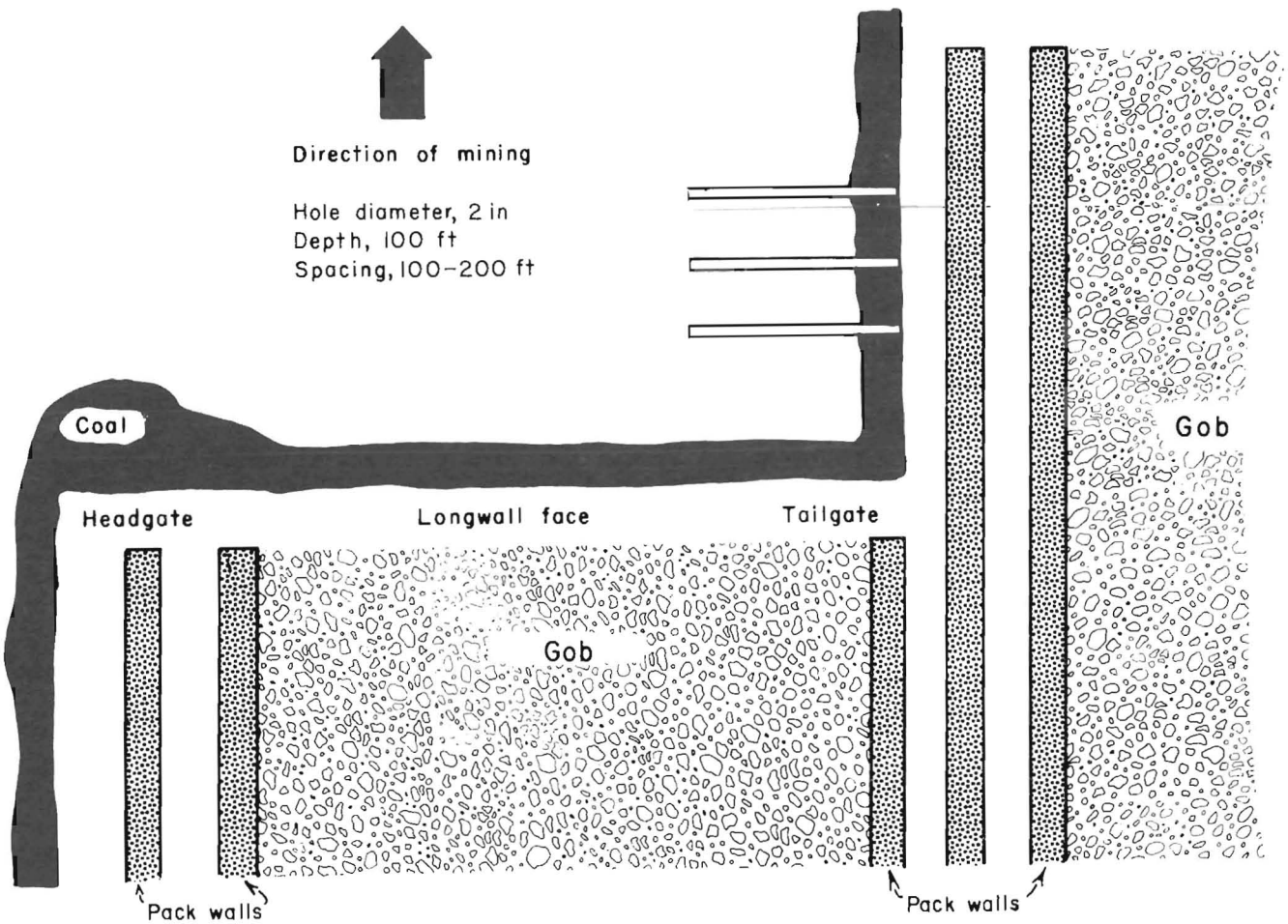


**Figure 19.—Hydraulic fracturing pattern ahead of longwall face.**

hydraulic fracturing. Fracturing a very large and highly stressed area causes loads to be redistributed and may create bump conditions in the mine.

### Auger Drilling

In this method, stress relief is induced by drilling holes into a highly stressed area. Depending on the magnitude of the stress, a hole or series of holes in a coal seam will structurally weaken the seam and cause failure of the coal; stress buildup cannot occur once the coal has failed. In 1958, Talman (*37*) reported experiences with large-diameter auger-drilled holes as a stress-relief method. The holes were 6 in. in diameter and maintained not less than 33 ft ahead of the face. The drill was positioned approximately 50 ft from the face, and barricades were constructed between the drill and the coal face. Violent bumps were triggered during drilling; however, mine personnel were protected by the barricades. In addition, the auger-drilling operation was performed on nonproduction shifts to minimize the number of workers present in the mine.

Long boreholes (50 to 80 ft) with large diameters (4.5 to 12 in), spaced on 13- to 16-ft centers, have been used to relieve stress at mining faces in foreign mines (*34–35*). The relationship among hole diameter, number of boreholes, and relief depends on conditions at each mine. In the United Kingdom, for instance, the borehole length does not exceed 30 ft, even for a 2- to 3-in-diam hole. In France and Belgium, the spacing between holes on the longwall face is 10 to 16 ft. In development entries, a fan-shaped pattern with five boreholes is drilled in the direction of advance (*36*). The maximum possible borehole diameter depends on the sensitivity of the seam or location being drilled; violent occurrences during drilling require the use of smaller diameter holes.

Experience in European coal mines, as well as conclusions from Talman (*37*), have shown that drilling from a distance, even for small-diameter boreholes, is required to safely drill in areas that are highly stressed. Furthermore, two adjacent holes should not be drilled simultaneously.

## LABORATORY INVESTIGATION OF ADSR

The auger drilling stress relief (ADSR) method was analyzed in a controlled setting using laboratory tests (*38*). The tests involved drilling different-diameter drill holes into triaxially loaded cubes to determine the combination of applied stress and drill hole size that would produce failure of the cube.

The test apparatus consisted of a steel test frame that allowed compressive vertical loading in a hydraulic press, while confining pressure was applied to all sides by hydraulic flatjacks. The cubes were first subjected to a vertical load of approximately 10,000 lb, with approximately 500 psi confining pressures. Holes were then drilled into the loaded cubes still in the apparatus, after which the vertical load was increased to cause material failure. The vertical load that caused failure of the cube was recorded for different hole diameters drilled. The results (fig. 20) show a definite relationship between the magnitude of the applied stress and the diameter of the drill hole that causes the specimen to fail. For highly stressed areas, a small drill hole can produce failure and, hence, stress relief. The question still remains: How large should the hole be, given the uncertainty regarding the exact magnitude of the stress abutment ahead of the face and other variables? The answer to this question requires in-mine experiments to determine the optimum solutions for each site-specific location; these local conditions and experience will dictate the selection of hole size, depth, and spacing.

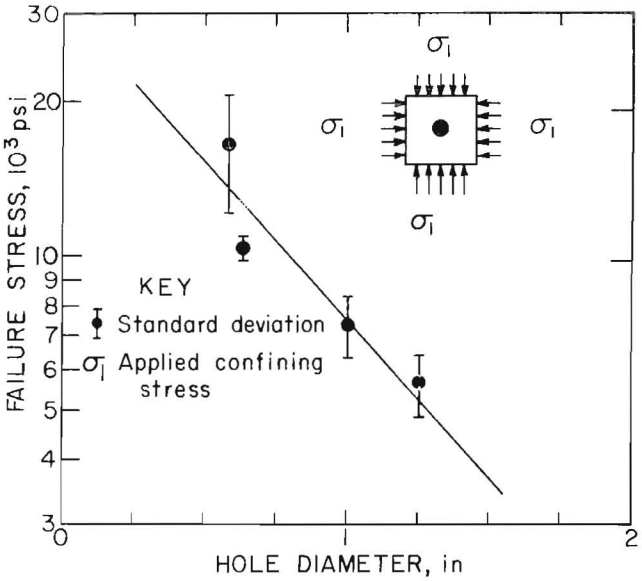


**Figure 20.—Relationship between failure stress magnitude and hole diameter causing failure.**

## NUMERICAL MODELING ANALYSIS

Computer model analysis was used to evaluate stress redistribution patterns resulting from destressing a longwall face. Model analyses focused on the test site longwall panel. The initial structural analysis used a two-dimensional finite-element model to provide an understanding of the pressure abutment surrounding the longwall panel and to provide a prediction of the weakened zone ahead of the longwall face (*38*). However, to simulate the true stress redistribution patterns caused by destressing, it was necessary to expand the analysis using the three-dimensional MULSIM model.

### Finite-Element Analysis

A two-dimensional finite-element model analysis of the longwall panel performed was represented by a vertical plane passing through sections A–A′ of figure 21. Figures 22 and 23 show details of the finite-element mesh.

Using symmetry, the model represented the mine conditions after 1,700 ft of face advance. The grid was matched to the actual geologic column of the mine site and extended 1,000 ft above and below the seam. Horizontally, the model included 800 ft of coal ahead of the face, 10 ft of supported roof at the shields, and 840 ft of gob. The seam being mined, the coal seam underlying the seam mined, and the sandstone parting between the coal seams were modeled, assuming a 10-ft thickness for each strata layer. All data used were representative of actual mining conditions. These data included mine geometry, coal and rock properties, and in situ stress conditions existing at the mine. Based on stress relief measurements

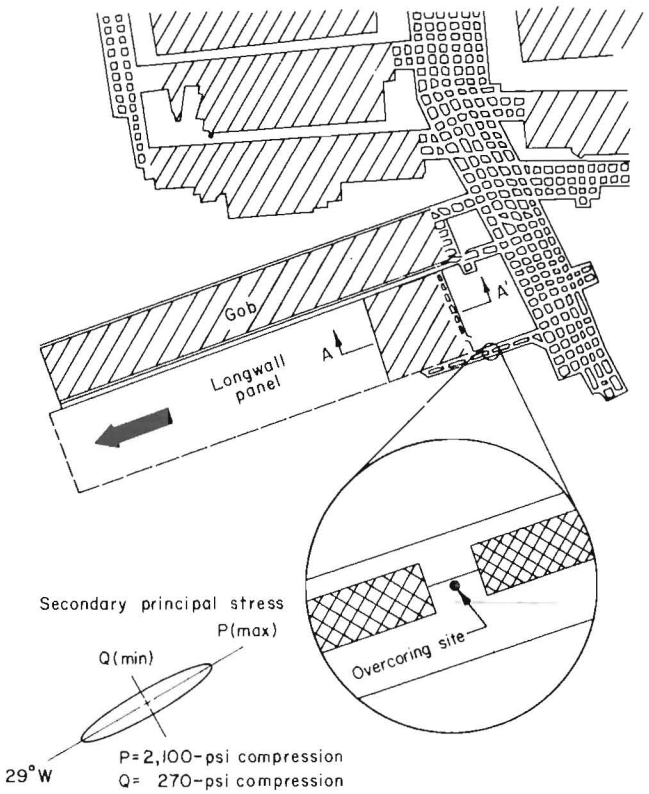


**Figure 21.—Finite-element model analysis represented by the vertical plane passing through line A–A'.**

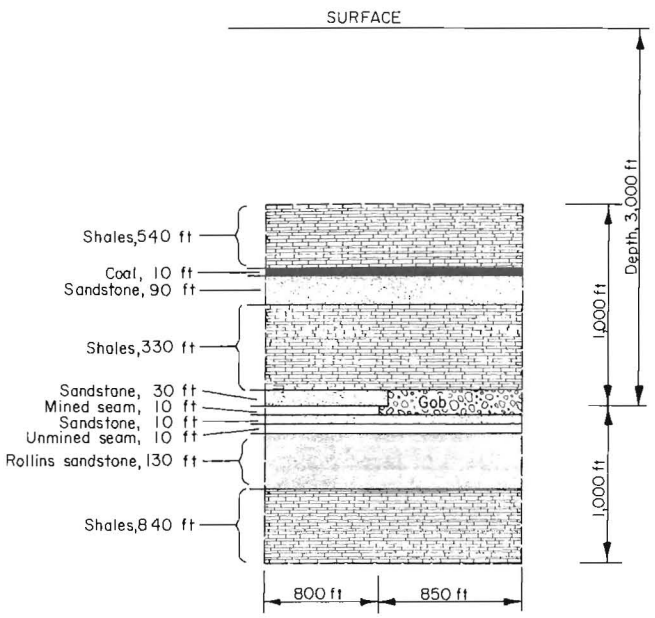


**Figure 22.—Conceptual finite-element model drawing.**

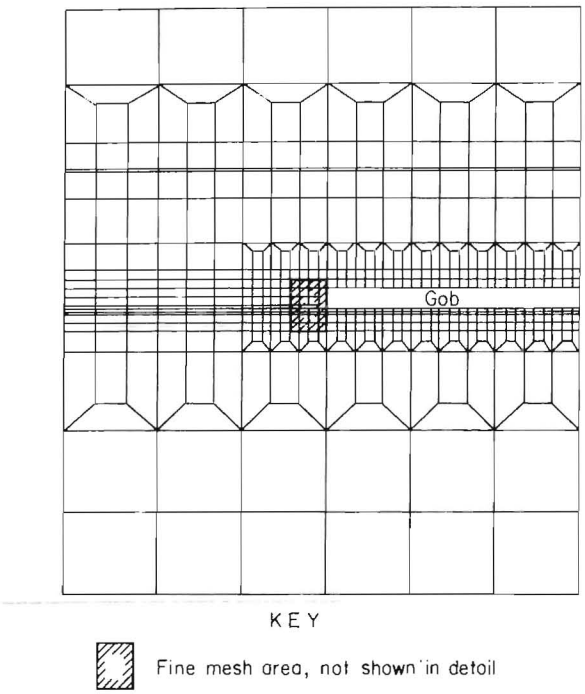


**Figure 23.—Finite-element mesh.**

from overcoring, the maximum horizontal stress was approximately 2,100 psi. Therefore, the model was run using a horizontal stress ($\sigma_h$) value of 0.7 psi/ft of depth. The modeled vertical stress ($\sigma_v$) was a standard overburden load value of 1.1 psi/ft of depth. These loading conditions established virgin stress conditions at the mine production horizon of $\sigma_v$ = 3,300 psi and $\sigma_h$ = 2,100 psi.

The in situ rock properties used in the model were selected to reflect actual mine conditions, which differ from those obtained using laboratory test samples. Based on previous MULSIM modeling experience (*20*), further adjustments were made to the strata properties immediately above the gob zone. The rock property modulus values were reduced to 10 pct of the normal effective in situ values in the first 60 ft above the gob zone. For the next 120 ft above the gob zone, the modulus values were reduced to 40 pct of the normal effective in situ values. Table 2 shows the elastic material properties used in the finite-element model.

## Finite-Element Analysis Results

The two-dimensional finite-element models provided results for the degree of partial yielding in the coal seam ahead of the longwall face, the size and location of the front abutment stress, and the effect of stresses in the sandstone parting below the mined seam.

Two cases were analyzed, differing only in the value used for the gob nonlinear stiffness parameters. Results for both cases showed that partial yielding in the coal seam occurred 10 to 20 ft ahead of the face. As a result, residual coal strength in the yielded region was about 50 pct of the original value. The front abutment stress was located approximately 20 ft ahead of

**Table 2.—Material properties used in finite-element model**

| Stratum | Poisson's ratio | Young's modulus, $10^6$ psi | Modeled effective Young's modulus, $10^6$ psi |
|---|---|---|---|
| Upper shales | 0.15 | 0.45 | 0.17 |
| Coal | .30 | .30 | .23 |
| Sandstone | .15 | 2.00 | .77 |
| Main roof: | | | |
| 100 pct stiffness | .15 | .45 | .17 |
| 40 pct stiffness | .15 | .18 | .07 |
| 10 pct stiffness | .15 | .04 | .02 |
| Immediate roof | .16 | 3.90 | 1.60 |
| Mined coal seam | .30 | .48 | .37 |
| Floor | .21 | 3.50 | 1.90 |
| Lower seam | .32 | .53 | .44 |
| Rollins sandstone | .16 | 2.70 | 1.10 |
| Subfloor | .15 | .45 | .17 |

NOTE.—Modeled effective Poisson's ratio was 0.39 for all strata.

the face, and the magnitude of the front abutment pressure was approximately seven times the overburden pressure. The rock parting was subjected to stresses sufficient to cause failure over an area beginning at 10 ft ahead of the face and extending 500 ft behind the face. These results are in agreement with the floor heave in the actual mine tailgate entries. All results are shown in figure 24.

## MULSIM Analysis

The thrust of the analysis was then changed to use the three-dimensional MULSIM program to analyze the transfer of stresses around failed or destressed zones. A modified version of MULSIM (*39*) was used. The modified version made it possible to include the effects of gob zones and accommodate inclusion of packwalls, cribs, and other artificial structural elements introduced into the seam. With these new capabilities in place, MULSIM was used to analyze

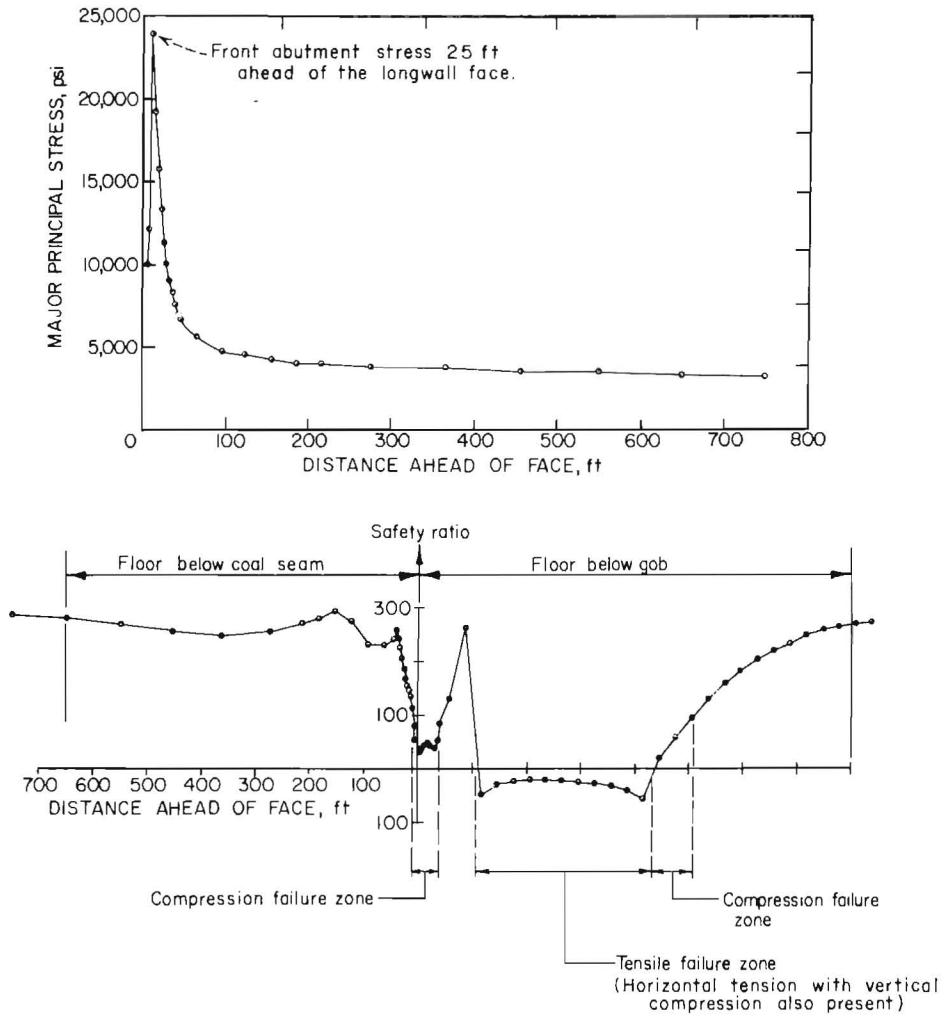


**Figure 24.—Vertical stress profiles in coal seam and floor.**

destressing options for an advancing longwall panel under circumstances similar to those of the test site. Using the location and magnitude of the front abutment stress from the finite-element results, a baseline model was created to fit these conditions.

The 600- by 600-ft baseline model shown in figure 25 represents a plan view of the longwall panel. Although the actual panel width is 800 ft, only 280 ft could be modeled within the available MULSIM grid size. All cases used 10-ft-wide elements. The modeled packwalls were 10 ft wide. The modeled material properties used for all cases are shown in table 3. These properties are based on in situ and laboratory measurements.

**Table 3.—Material properties used in MULSIM model**

| Material type | Young's modulus, $10^6$ psi | Poisson's ratio |
|---|---|---|
| Rock mass | 0.384 | 0.15 |
| Intact coal | .480 | .30 |
| Weakened coal | .240 | .30 |
| Destressed coal | .005 | .40 |
| Gob[1] | .005 | .40 |
| Pack walls: | | |
| Case A | 2.500 | .13 |
| Other cases | .250 | .13 |

[1]Since MULSIM gob height is limited to the seam height, this value is equivalent to a modulus of 137.89 MPa (20,000 psi) for a gob whose height is 4 times the seam height.

A stiffness value for weakened coal was set at one-half the stiffness of the intact coal. This reduction was based on the finite-element results, which showed a yield factor of at least 0.5 for coal within 10 ft of the longwall face. The properties for destressed coal were arbitrarily selected to represent low residual stiffness.

The modeled state of stress used to represent mine conditions was as follows:

$$\sigma_v = 1.1 \text{ psi/ft} \cdot D, \quad (8)$$

$$\sigma_{h1} = 0.7 \text{ psi/ft} \cdot D, \quad (9)$$

$$\sigma_{h2} = 0.05 \text{ psi/ft} \cdot D, \quad (10)$$

where $\sigma_v$ = vertical stress, psi,
$\sigma_{h1}$ = horizontal stress parallel to the longwall advance, psi,
$\sigma_{h2}$ = horizontal stress parallel to the longwall face, psi,
and $D$ = depth, ft.

## MULSIM Analysis Results

After the baseline case was selected, eight other cases were modeled to analyze the effect of various possible face destressing patterns. The analysis ranged from destressing of a small isolated area to the destressing of the entire modeled length of the longwall face. The column of weakened coal elements adjacent to the face was subdivided into 14 destressing zones of 2 elements each (fig. 25). Any zone, or combination of zones, could be modeled as destressed simply by changing the material type for the appropriate elements to destressed coal.

The eight cases studied, labeled D1 through D8, are shown in figure 26. For example, in cases D1 and D2, only isolated 40-ft sections of the face were destressed. For all cases, the zones not destressed were modeled using the material properties for weakened coal. Based on the finite-element

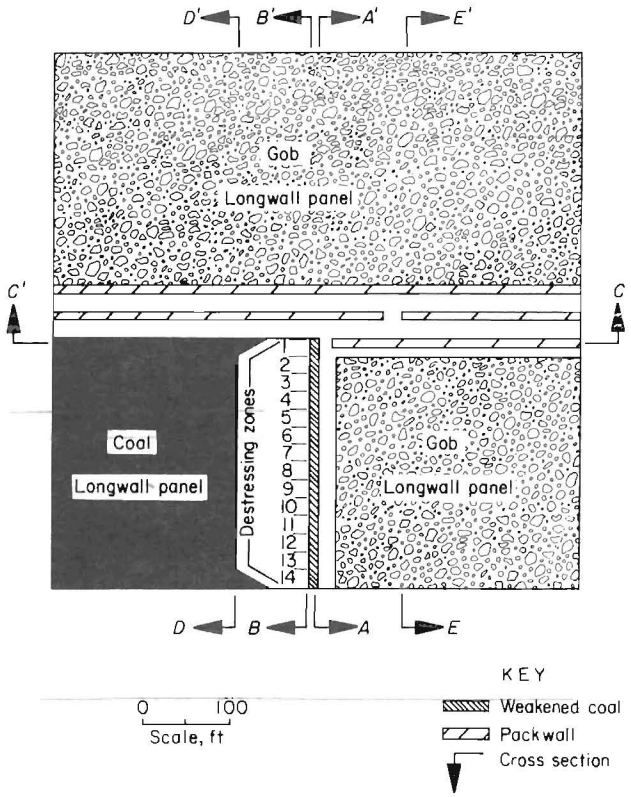


**Figure 25.—MULSIM grid cases D1 through D8.**

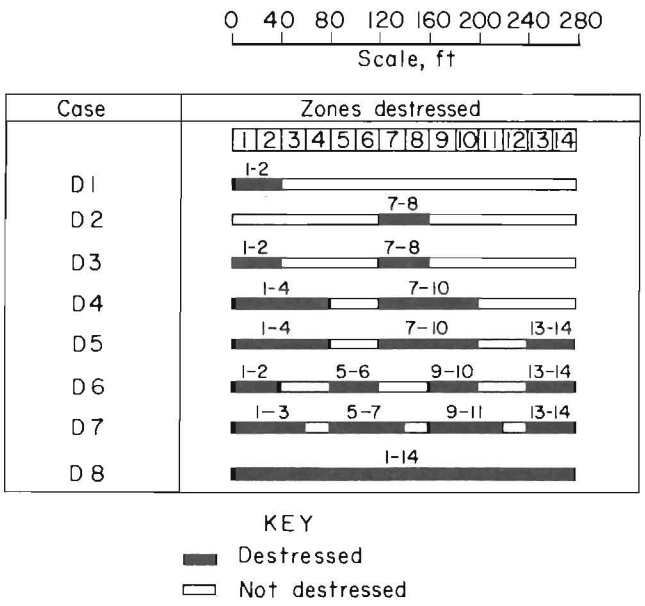


**Figure 26.—Zones destressed for cases D1 through D8.**

results, the depth of the destressed zone chosen was 10 ft, equivalent to the distance of the front abutment stress ahead of the longwall face.

Model results for each destressing case were reduced to the form of graphs of the calculated distribution of vertical stresses in the seam. Vertical stresses were plotted for cross sections A–A′ and B–B′. In figure 25, line A–A′ represents the stress profile on the face, and line B–B′ represents the stress profile approximately 15 ft ahead of the face. The vertical stress distribution for lines A–A′ and B–B′ for all cases are illustrated in figure 27.

In general, the MULSIM analysis results showed that destressing a portion of the face redistributed the stresses from the destressed areas to adjacent locations that were not destressed ahead of the face. This effect results in high-stress peaks on the face in areas adjacent to the destressed zones. Table 4 summarizes the stress redistribution in the form of stress increase factors for stresses in locations adjacent to the destressed area as compared with the corresponding stresses from the baseline case.

**Table 4.—Stress increase adjacent to destressed areas**

| Case | Location of comparison, ft | New stress location, psi | Increase factor from baseline |
|---|---|---|---|
| CROSS SECTION A–A′ | | | |
| D1 | 275 | 21,000 | 1.4 |
| D2 | 145 | 16,500 | 1.5 |
| D3 | 145 | 16,500 | 1.5 |
| D4 | 115 | 17,500 | 1.7 |
| D5 | 125 | 18,000 | 1.7 |
| D6 | 105 | 17,000 | 1.6 |
| D7 | 85 | 18,000 | 1.7 |
| D8 | 275 | 22,000 | 1.5 |
| CROSS SECTION B–B′[1] | | | |
| D1 | 235 | 19,000 | 1.2 |
| D2 | 165 | 19,500 | 1.2 |
| D3 | 165 | 19,500 | 1.2 |
| D4 | 165 | 20,500 | 1.3 |
| D5 | 75 | 21,000 | 1.3 |
| D6 | 235 | 19,500 | 1.3 |
| D7 | 125 | 21,000 | 1.3 |

[1]No data available for case D8, section B–B′.

The simulated destressing caused maximum stress increase factors in nearly all locations ranging from 1.4 to 1.7 along line A–A′ and from 1.2 to 1.3 along line B–B′. The larger increases for each of the two sections occurred primarily for cases D4, D5, and D7, in which the majority of the face was destressed while smaller regions were left intact to carry increased stresses. In all eight cases, stresses adjacent to the face increased beyond the previous abutment peak values in any regions that were not destressed. Destressing the entire face, however, resulted in a stress increase of 1.5 times the previous abutment stress at 15 ft ahead of the face, while a drop in the stress at the face was noticed.

Vertical stress plots were also developed for each case at 100 ft ahead along line D–D′ and 100 ft behind the face along line E–E′. No stress changes due to destressing were indicated at these points.

Dangerous high-stress conditions may occur if portions of the longwall face are destressed while isolated areas are left untreated. The lowest attainable stress levels adjacent to the face of the panel are achieved by destressing the entire face, as in case D8.

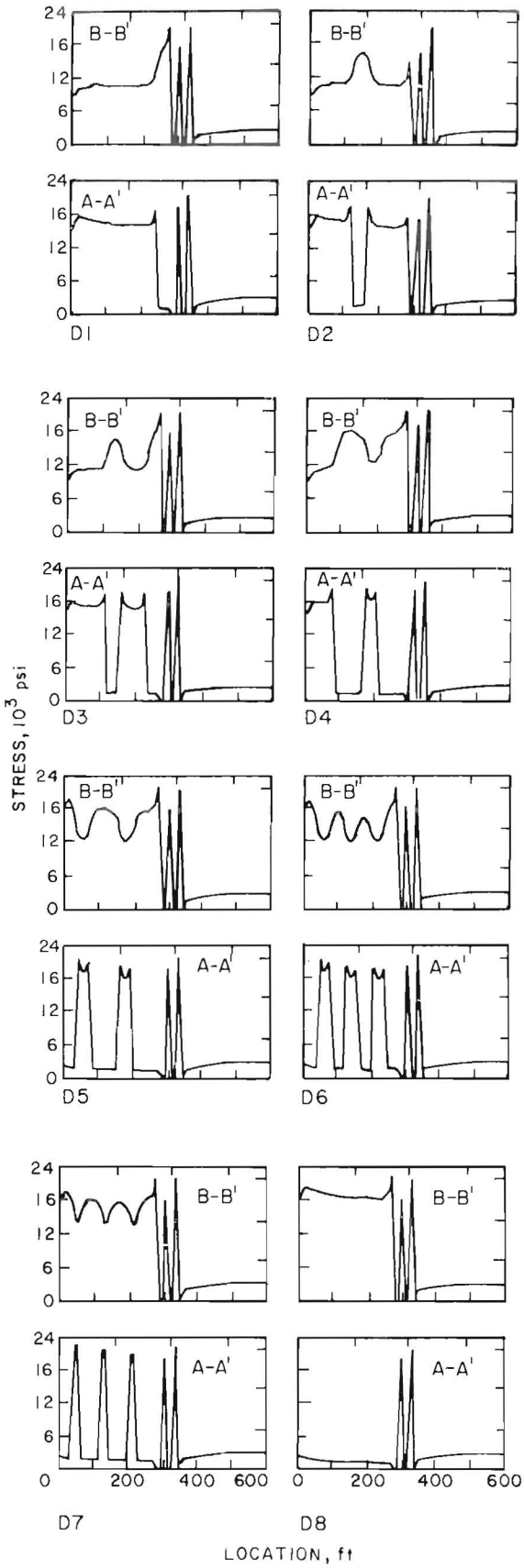


**Figure 27.—Vertical stress profiles for lines A–A′ and B–B′ for cases D1 through D8.**

A stress distribution plot along cross section C–C′ for case D8 indicates that a stress abutment extended approximately 100 ft adjacent to the tailgate entry in advance of the longwall face. Although no cases were run to confirm the effects of this recommendation, it would be clearly desirable to destress the panel for at least 100 ft alongside the entry. Any of the three destressing methods discussed might be effective. One possible method could be hydrofracturing, using a system of drill holes approximately 75 to 100 ft ahead of the face. Auger-drilling patterns or volley-firing patterns may also be effective ways to produce the indicated stress relief.

# ROCK MECHANICS INVESTIGATION

Since high-stress zones are a common denominator in the bump problem, a better understanding of the causes of high-stress concentration and stress redistribution during mining should lead to the development of control techniques to alleviate the strata pressures or to trigger bumps in a controlled fashion. Based on this rationale, an instrumentation program was developed to monitor stress changes, roof and floor deformations, and shield loading in a bump-prone mine. The data will be used to evaluate the following:

- Causes and location of high-stress concentrations;
- Relationship of bump occurrences to stress distributions;
- Development of systematic methods to prevent or control coal mine bumps.

## DATA COLLECTION

Different types of rock mechanics data were collected.

1. Stress:
   a. Magnitude and direction of the secondary horizontal principal stresses.
   b. Stress redistribution caused by mining.
   c. Shield loading.
2. Strata movement:
   a. Roof separation.
   b. Roof-floor convergence.
   c. Panel-rib expansion.
3. Geotechnical data:
   a. Coal-rock properties.
   b. Geological mapping.

Based on the need to gather data before and after a bump, all instruments were installed prior to advancing the longwall face. Shield pressure data collection did not begin until the face advanced about 150 ft.

## INSTRUMENTATION

1. *Stress*

a. The magnitude and direction of the maximum and minimum secondary principal horizontal stresses were obtained using the Bureau overcoring technique with the three-component borehole deformation gauge. Overcoring was performed in the roof of the longwall headgate entry approximately 250 ft inby the longwall starting room (fig. 21). A vertical borehole was drilled about 9 ft into the roof before proceeding with overcoring tests, so the tests would not be influenced by stress concentration surrounding the mine openings. A total of four reliefs at 16-in intervals were collected; however, cores from only two reliefs were used since the other two cores fractured during recovery. The maximum principal horizontal stress, approximately 2,100 psi in compression, was measured parallel to the headgate entry axis.

b. Borehole pressure cells (BPC's) were installed in the panel and pack walls at two stations in the tailgate entries and were oriented to measure vertical stress changes during mining. Stations 1 and 2 were located 950 ft and 2,000 ft inby the longwall starting room, respectively. Three BPC's were installed in each packwall. The cells were located approximately 2 ft from the packwall edges and in the packwall core. The BPC's in the panel were installed on approximately 5-ft intervals up to 20 ft from the rib and on 10-ft intervals between 20 and 50 ft in the panel. Each BPC was initially pumped to a setting pressure of 3,000 psi, approximately the premining overburden pressure based on 3,000 ft of overburden. No cells were installed at depths greater than 60 ft because drilling into the panel became difficult at this depth. The instrumentation plans for both stations are shown in figure 28.

c. The hydraulic pressure on each leg of seven different shields was continuously recorded using mechanical chart recorders with a range from 0 to 10,000 psi. The shields numbered 5, 24, 44, 57, 84, 144, and 155 were monitored. Each shield is approximately 5 ft wide, and the shields are numbered from the headgate to the tailgate starting with number 1 in the headgate entry. Mining height at the face was recorded to the nearest 0.1 ft when the shield pressure charts were changed.

2. *Strata Movement*

a. Multipoint borehole extensometers (MPBX) were installed in the roof in the upper and lower tailgate entries at stations 1 and 2 to detect movements at different heights in the roof. The anchor depths were selected to coincide with the various geologic roof layers. Because of the existence of a strong sandstone layer in the roof, roof layer separations were minimal; anchor depths are illustrated in figure 28. Four-point

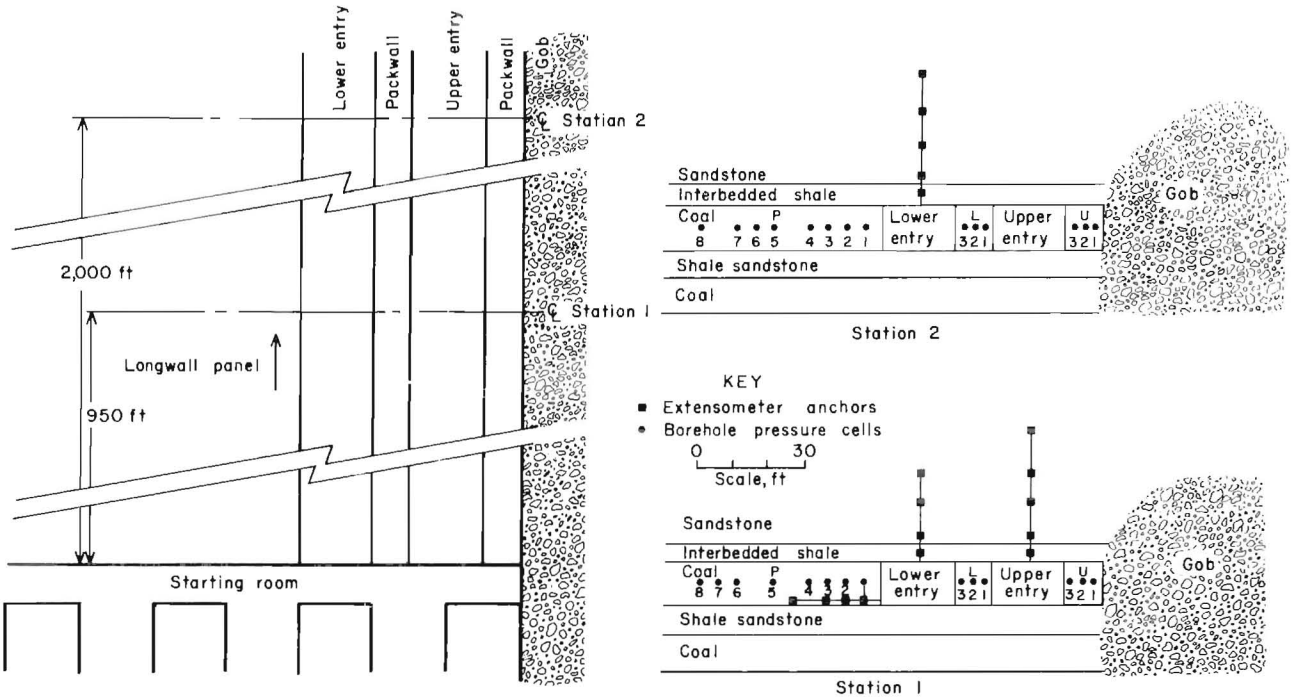


**Figure 28.—Instrumentation plan for stations 1 and 2.**

extensometers with anchors located at 5, 10, 15, and 20 ft from the rib were also installed in the longwall panel at station 1 to measure the lateral deformation of coal as mining advanced. Readings from the MPBX were recorded to the nearest 0.001 in.

b. Thirty-five roof-to-floor convergence stations were installed on 50-ft intervals along the lower tailgate entry. The first station was installed 450 ft ahead of the starting room, and the last station was at 2,000 ft ahead of the starting room. Each convergence station consisted of a 3/4-in-diam by 22-in-long steel reinforcing rod grouted in a 1-5/8-in-diam borehole drilled in the floor directly beneath a roof bolt. A rod-type extensometer was used to measure the distance between the bolt head and the rod in the floor. The extensometer reads directly to the closest 0.01 in. The floor rods were installed at a depth of about 20 in to provide a solid anchorage in the floor.

3. *Geotechnical Data*

a. Physical property testing was performed on core samples obtained from two NX-size holes drilled into the roof and floor of the third crosscut in the headgate entry. NX-size core diameter is 2-⅛-in. Core samples up to 32 ft above and 36 ft below the mined seam were recovered and tested in the laboratory. Table 5 shows the uniaxial and triaxial test results from the roof, floor, and coal samples. Table 6 shows the Brazilian test results.

Thirty in situ borehole shear strength tests were performed at 2- to 3-ft intervals in the roof and 1- to 2-ft intervals in the floor. Data from a borehole shear tester (BST) are used to obtain in situ values of angle of internal friction ($\phi$) and cohesion ($S_o$) (*40*). Using the BST results, the in situ uniaxial compressive strength ($\sigma_c$) and the in situ rock tensile strength ($\tau_o$) were calculated applying the following equations (*41*); results are presented in table 7.

$$\sigma_c = \frac{2\ S_o\ \mathrm{Cos}\ \phi}{1 - \mathrm{Sin}\ \phi} \tag{11}$$

and

$$\tau_o = \frac{2\ S_o}{\tan\ \phi + [(\tan\ \phi)^2 + 1]^{1/2}}, \tag{12}$$

where $\sigma_c$ = in situ compressive strength, psi,
$\tau_o$ = in situ tensile strength, psi,
$\phi$ = angle of internal friction from BST, deg,
and $S_o$ = cohesion from BST, psi.

**Table 5.—Uniaxial and triaxial test results from roof, floor, and coal**

| Depth or sample | Length, in | Specific gravity | Lateral pressure, psi | Breaking load, lb | Compressive strength, psi | Young's modulus, $10^6$ psi | | Poisson's ratio | |
|---|---|---|---|---|---|---|---|---|---|
| | | | | | | Tangent | Secant | Tangent | Secant |
| ROOF ROCK[1] | | | | | | | | | |
| 9 ft 3 in to 9 ft 7 in ..... | 4.285 | 2.564 | 500 | 89,500 | 24,767 | 4.298 | 3.986 | | |
| 9 ft 7 in to 9 ft 11 in.... | 4.285 | 2.574 | 500 | 91,800 | 25,404 | 4.638 | 3.869 | | |
| 11 ft 4 in to 11 ft 8 in.. | 4.305 | 2.531 | 1,000 | 86,000 | 23,799 | 3.486 | 3.229 | | |
| 11 ft 8 in to 12 ft..... | 3.908 | 2.543 | 1,000 | 79,000 | 21,862 | 3.437 | 3.279 | | |
| 19 ft 4 in to 19 ft 8 in.. | 4.275 | 2.613 | 1,000 | 57,000 | 15,774 | 2.455 | 2.213 | | |
| 19 ft 8 in to 20 ft 0 in.. | 4.280 | 2.629 | 1,500 | 72,500 | 20,063 | 2.657 | 2.431 | | |
| 20 ft 10 in to 21 ft 2 in. | 4.244 | 2.608 | 1,500 | 71,900 | 19,897 | 2.390 | 2.390 | | |
| 24 ft 0 in to 24 ft 4 in.. | 4.283 | 2.648 | 0 | 74,500 | 20,616 | 4.009 | 3.384 | 0.132 | 0.05 |
| 24 ft 4 in to 24 ft 8 in.. | 4.280 | 4.689 | 0 | 81,800 | 22,636 | 5.704 | 5.140 | .142 | .141 |
| 24 ft 8 in to 25 ft 1 in.. | 4.280 | 2.706 | 0 | 107,000 | 29,610 | 6.102 | 5.751 | .206 | .175 |
| FLOOR ROCK[1] | | | | | | | | | |
| 6 ft 3 in to 6 ft 7 in ..... | 4.285 | 2.615 | 0 | 21,200 | 5,867 | 1.611 | 0.957 | 0.115 | 0.051 |
| 8 ft 0 in to 8 ft 4 in ..... | 4.260 | 2.671 | 500 | 119,000 | 32,931 | 5.505 | 5.505 | | |
| 9 ft 8 in to 10 ft 0 in.... | 4.301 | 2.575 | 0 | 37,700 | 10,443 | 3.257 | 2.785 | .313 | .221 |
| 21 ft 0 in to 21 ft 5 in.. | 4.301 | 2.209 | 0 | 14,700 | 4,068 | .585 | .376 | .151 | .087 |
| 22 ft 3 in to 22 ft 7 in.. | 3.948 | 2.424 | 500 | 29,800 | 8,247 | 1.300 | 1.300 | | |
| 30 ft 6 in to 30 ft 10 in.. | 4.300 | 2.493 | 1,000 | 70,500 | 19,509 | 3.364 | 3.251 | | |
| 31 ft 6 in to 31 ft 10 in. | 4.280 | 2.513 | 1,000 | 72,200 | 19,980 | 3.535 | 3.055 | | |
| 34 ft 8 in to 35 ft 0 in.. | 4.295 | 2.460 | 1,500 | 82,000 | 22,692 | 4.079 | 3.121 | | |
| COALBED BELOW FLOOR ROCK[2] | | | | | | | | | |
| 1 ..... | 3.970 | 1.490 | 0 | 8,300 | 2,351 | 0.551 | 0.453 | 0.291 | 0.230 |
| 2 ..... | 3.950 | 1.540 | 0 | 5,700 | 1,615 | .442 | .342 | .164 | .093 |
| 3 ..... | 3.955 | 1.694 | 0 | 11,800 | 3,343 | .556 | .441 | .490 | .441 |
| 4 ..... | 3.965 | 1.500 | 250 | 11,600 | 3,286 | .662 | .662 | | |
| 5 ..... | 3.965 | 1.311 | 250 | 8,000 | 2,266 | .417 | .382 | | |
| MINED COALBED[1] | | | | | | | | | |
| 1 ..... | 3.970 | 1.118 | 250 | 12,400 | 3,513 | 0.470 | 0.461 | | |
| 2 ..... | 3.912 | 1.078 | 500 | 6,250 | 1,771 | .289 | .289 | | |
| 3 ..... | 3.889 | 1.127 | 500 | 12,500 | 3,541 | .429 | .362 | | |
| 4 ..... | 3.908 | 1.184 | 500 | 14,700 | 4,164 | .486 | .434 | | |
| 5 ..... | 3.904 | 1.069 | 750 | 16,300 | 4,618 | .481 | .362 | | |
| 6 ..... | 3.893 | 1.073 | 750 | 18,300 | 5,184 | .502 | .347 | | |
| 7 ..... | 3.900 | 1.065 | 750 | 16,700 | 4,731 | .488 | .356 | | |
| 8 ..... | 3.905 | 1.076 | 1,000 | 19,250 | 5,453 | .495 | .340 | | |
| 9 ..... | 3.918 | 1.057 | 1,000 | 15,700 | 4,448 | .427 | .330 | | |
| 10 ..... | 3.912 | 1.070 | 1,000 | 21,700 | 6,147 | .689 | .401 | | |
| COALBED BELOW FLOOR ROCK[3] | | | | | | | | | |
| 1 ..... | 1.958 | 1.472 | 0 | 7,500 | 2,125 | 0.412 | 0.344 | 0.394 | 0.214 |
| 2 ..... | 1.952 | 1.314 | 0 | 6,800 | 1,926 | .331 | .201 | .351 | .144 |
| 3 ..... | 1.960 | 1.587 | 0 | 14,400 | 4,079 | .592 | .340 | .265 | .152 |
| MINED COALBED[4] | | | | | | | | | |
| 1 ..... | 1.975 | 1.071 | 0 | 4,900 | 1,641 | 0.312 | 0.256 | 0.407 | 0.192 |
| 2 ..... | 1.975 | 1.115 | 0 | 9,800 | 3,281 | .395 | .175 | .393 | .146 |
| 3 ..... | 1.975 | 1.069 | 0 | 3,800 | 1,272 | .298 | .184 | .564 | .206 |
| 4 ..... | 1.975 | 1.062 | 0 | 3,600 | 1,205 | .239 | .155 | .639 | .291 |
| 5 ..... | 1.975 | 1.075 | 0 | 3,450 | 1,155 | .137 | .054 | .317 | .097 |

[1]Sample length-to-diameter ratio = 2, diameter = 2.145 in.
[2]Sample length-to-diameter ratio = 2, diameter = 2.120 in.
[3]Sample length-to-diameter ratio = 1, diameter = 2.120 in.
[4]Sample length-to-diameter ratio = 1, diameter = 1.950 in.
NOTE.—Blank spaces under Poisson's ratio indicate Poisson's ratio is not measured when lateral pressure is applied to the sample.

**Table 6.—Brazilian test results of cores from roof and floor rock**

| Depth | Length, in | Specific gravity | Breaking load, lb | Indirect tensile strength, psi |
|---|---|---|---|---|
| | | ROOF ROCK[1] | | |
| 2 ft 0 in to 2 ft 2 in ..... | 2.161 | 2.543 | 3,040 | 422 |
| 5 ft 9 in to 5 ft 11 in.... | 2.160 | 2.681 | 10,730 | 1,492 |
| 6 ft 3 in to 6 ft 5 in ..... | 2.167 | 2.650 | 6,660 | 923 |
| 7 ft 8 in to 7 ft 10 in.... | 2.168 | 2.665 | 5,520 | 764 |
| 8 ft 0 in to 8 ft 2 in ..... | 2.013 | 2.654 | 12,070 | 1,800 |
| 8 ft 2 in to 8 ft 4 in ..... | 2.157 | 2.693 | 7,150 | 995 |
| 18 ft 10 in to 19 ft 0 in. | 2.173 | 2.490 | 8,190 | 1,131 |
| 20 ft 4 in to 20 ft 6 in.. | 2.165 | 2.540 | 5,525 | 766 |
| 31 ft 4 in to 31 ft 6 in.. | 2.182 | 2.514 | 8,760 | 1,206 |
| 31 ft 7 in to 31 ft 9 in.. | 2.178 | 2.660 | 12,140 | 1,674 |
| | | FLOOR ROCK[2] | | |
| 2 ft 0 in to 2 ft 2 in ..... | 2.165 | 2.605 | 3,730 | 510 |
| 5 ft 3 in to 5 ft 6 in ..... | 2.158 | 2.612 | 7,200 | 987 |
| 7 ft 0 in to 7 ft 3 in ..... | 2.133 | 2.566 | 8,740 | 1,213 |
| 7 ft 3 in to 7 ft 6 in ..... | 2.174 | 2.627 | 10,970 | 1,494 |
| 8 ft 4 in to 8 ft 7 in ..... | 2.158 | 2.607 | 9,090 | 1,247 |
| 10 ft 1 in to 10 ft 3 in.. | 2.156 | 2.612 | 4,010 | 550 |
| 10 ft 4 in to 10 ft 7 in.. | 2.167 | 2.616 | 9,130 | 1,248 |

[1]Sample length-to-diameter ratio = 1, diameter = 2.120 in.
[2]Sample length-to-diameter ratio = 1, diameter = 2.150 in.

**Table 7.—In situ physical properties from borehole shear test results**

| Test depth, ft | Friction angle, deg | Cohesion, psi | Uniaxial compressive strength, psi | Tensile strength, psi |
|---|---|---|---|---|
| | | ROOF | | |
| 3 ..... | 37.3 | 176 | 711 | 175 |
| 6 ..... | 44.5 | 261 | 1,245 | 219 |
| 9 ..... | 38.9 | 61 | 255 | 58 |
| 12 ..... | 29.2 | 609 | 1,888 | 715 |
| 18 ..... | 33.4 | 51 | 189 | 55 |
| 21 ..... | 28.6 | 523 | 1,762 | 621 |
| 24 ..... | 36.1 | 447 | 1,758 | 455 |
| 27 ..... | 23.0 | 556 | 1,680 | 736 |
| 30 ..... | 39.1 | 9 | 38 | 9 |
| | | FLOOR | | |
| 1.5 ..... | 37.0 | 187 | 750 | 186 |
| 3 ..... | 26.0 | 773 | 2,474 | 966 |
| 4 ..... | 32.9 | 294 | 1,081 | 320 |
| 5 ..... | 29.4 | 409 | 1,400 | 478 |
| 6 ..... | 11.1 | 1,070 | 2,601 | 1,761 |
| 7 ..... | 28.5 | 611 | 2,054 | 727 |
| 8 ..... | 20.5 | 1,279 | 3,687 | 1,775 |
| 9 ..... | 35.4 | 368 | 1,426 | 380 |
| 11 ..... | 16.5 | 444 | 1,189 | 663 |
| 13 ..... | 14.1 | 517 | 1,326 | 806 |
| 15 ..... | 15.5 | 560 | 1,372 | 852 |
| 17 ..... | 23.0 | 308 | 931 | 408 |
| 19 ..... | 25.5 | 200 | 634 | 252 |
| 21 ..... | 20.1 | 478 | 1,368 | 668 |
| 23 ..... | 24.2 | 488 | 1,509 | 631 |
| 25 ..... | 28.0 | 376 | 1,252 | 452 |
| 27 ..... | 23.3 | 1,088 | 3,306 | 1,432 |
| 29 ..... | 35.4 | 489 | 1,895 | 505 |
| 31 ..... | 35.8 | 423 | 1,653 | 433 |
| 33 ..... | 35.6 | 308 | 1,199 | 317 |
| 35 ..... | 34.5 | 356 | 1,353 | 375 |

b. Two major faults were mapped crossing the studied longwall panel at approximately 3,900 ft from the starting room.

## DATA ANALYSIS

The primary emphasis of data collection and analysis was mainly directed toward characterizing roof caving, forward abutment pressure, and room closure influences on bumps.

### Roof Caving

Different methods to predict roof caving are available (*42*). One of the most common methods, used for this study, is recording the shield leg pressure and calculating the time-weighted average resistance (TWAR) during the periodic roof weighting. The time-weighted average pressure (TWAP) of each shield leg is the area under the pressure-versus-time curve recorded for each cycle divided by the total cycle time. Figure 29 shows a typical pressure-time curve for a shield leg during a mining cycle. The variation in hydraulic pressure results from the forces applied to the shields through the roof and floor. Initially, the shield is set against the roof, at point s. As the neighboring shields are lowered, advanced, and set, the pressure on the shield increases from point s to a. The increase in pressure from point a to b is caused by the excess shield loading due to mining. When the shearer is cutting in the immediate vicinity of the shield, an increase in the pressure from point b to c is noticed. As the adjacent supports are lowered, advanced, and set, a significant pressure increase occurs in the cycle shown from point c to d. Finally, as the shield is lowered so it can be advanced, the pressure drops from point d to e. Every shield cycle varies because of the interaction between the roof, floor, and shield, location of the shield with respect to face location, and changes in hydraulic pump pressure.

The TWAP was calculated for each shield leg using the following equation:

$$TWAP = \frac{1/2(P_a + P_s)t_a + 1/2(P_b + P_a)t_b + 1/2(P_c + P_b)t_c + 1/2(P_d + P_c)t_d}{t_a + t_b + t_c + t_d}. \quad (13)$$

Referring to figure 29, $P_a$, $P_b$, $P_c$, and $P_d$ are the pressures at points a, b, c, and d, respectively; $P_s$ is the shield setting pressure; $t_a$, $t_b$, $t_c$, and $t_d$ are the times at points a, b, c, and d, respectively.

TWAP gives a good indication of the amount of pressure in each shield leg. To calculate the TWAR on the shields in tons, the following equation was used:

$$TWAR = (\Sigma \text{ TWAP on both legs}) \cdot \frac{Ax}{2{,}000} \cdot e/f, \quad (14)$$

where TWAR = time-weighted average resistance, tons,
TWAP = time-weighted average pressure, psi,
$A_x$ = cross-sectional area of shield leg, $in^2$,
= $\pi D^2/4$, where D is the diameter of shield leg, in,
and e/f = leg efficiency specific to the support (dependent on mining height).

The calculated TWAR versus face distance, in tons for each shield, was plotted in figure 30. The average periodic weighting interval for all instrumented shields, which is the distance between the maximum TWAR, is approximately 40 ft. Data from shield 5, located approximately 25 ft from the headgate entry, indicate regular breaking and caving of the roof behind the face on the average of 40 ft; the peaks in the TWAR are spaced approximately 40 ft apart. Shields at the center of the panel also indicate fairly regular caving, but with an average periodic weighting interval of approximately 50 ft. Data from shields 144 and 155, which are very close to the tailgate entry, indicate that the roof was not caving regularly. In fact, the TWAR results indicate that a high-load cycle, which may result from noncaving of the tailgate roof, extended for a distance of approximately 145 ft of face advance prior to a major bump in April 20, 1983.

Analysis of the data shows that when the roof readily caves, the face is not overstressed and no major face bumps occur. Conversely, if, as the roof hangs as a cantilever beam behind the shields, the weight of the beam is transferred onto the coal, face bump conditions may exist. The exact cantilever length that causes the high-stress conditions is not easy to determine. The high-loading cycle, which extended 145 ft, contributed to the high-stress conditions, and even shorter cantilever lengths may have contributed to high-stress conditions near the middle of the face.

## Forward Abutment

Movement of the forward abutment as mining progressed was monitored by BPC's, roof-to-floor convergence stations, and MPBX's installed in the tailgate entry roof ahead of the face.

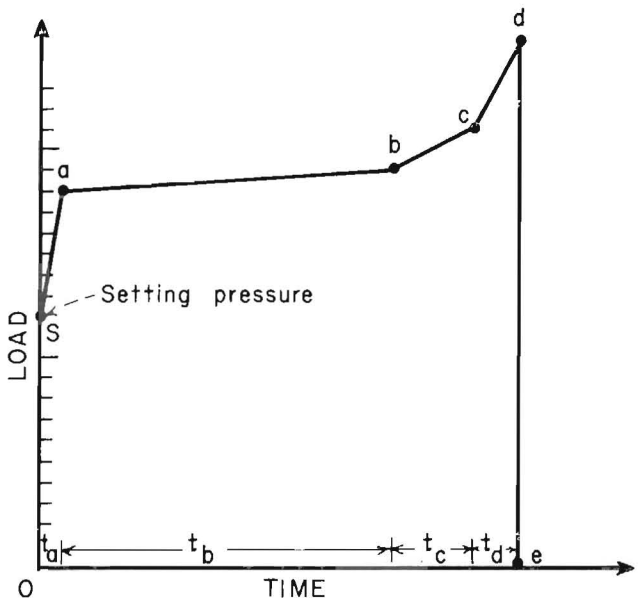


**Figure 29.—Typical pressure-time curve for shield leg during mining cycle (*46*).**

Figure 31 shows the effect of mining on the vertical pressure changes in the upper and lower packwalls. BPC's installed in the upper packwall adjacent to a previously mined longwall, U1 and U2, showed no significant changes as the face advanced, while data from cell U3 adjacent to the upper entry indicated a gradual pressure decrease with an average gradient of 2.5 psi/ft of face advance. In the lower packwall, however, cell L2 installed in the packwall core showed no significant pressure changes, and cells L1 and L3 adjacent to the upper and lower gate entries indicated a gradual pressure decrease with an average of 3.25 and 1.25 psi/ft, respectively.

This behavior may be caused by the loss of confinement under the packwalls due to floor heave in the entries. Cells U1 and U2 are not affected because the upper packwall is partially confined by the gob from the previously mined panel and loaded by continuing roof deflection toward the gob. Prior to the April 20 bump, all cells showed a decrease in pressure, while after the bump, all cells rebounded to the prebump pressure except cells U3 and L1, which did not regain the prebump pressure; this phenomenon is further evidence of the effect of floor heave on the packwall pressure.

Instrumentation at station 1 indicated the forward abutment extended approximately 570 ft ahead of the face (fig. 32).

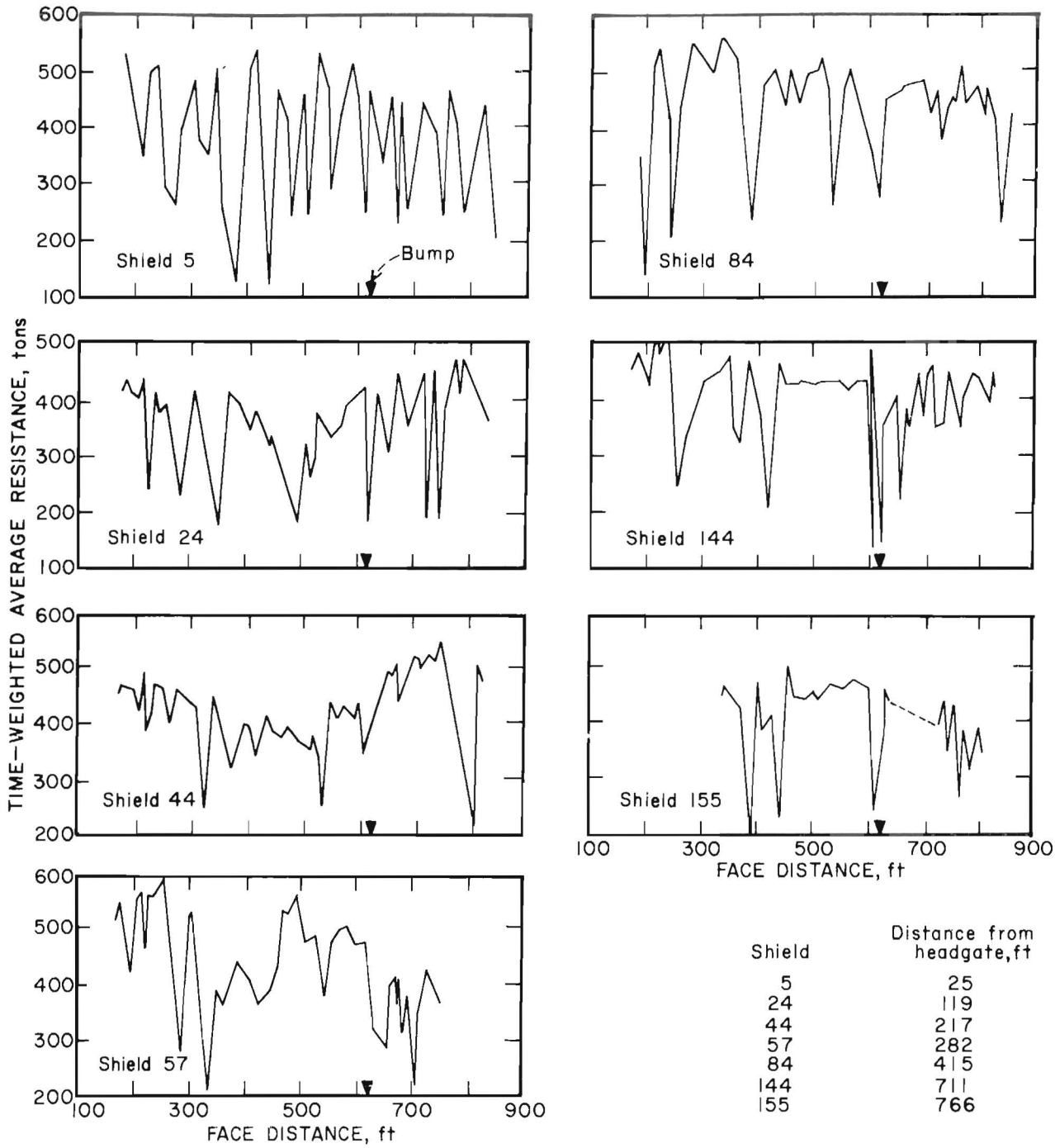


| Shield | Distance from headgate, ft |
|---|---|
| 5 | 25 |
| 24 | 119 |
| 44 | 217 |
| 57 | 282 |
| 84 | 415 |
| 144 | 711 |
| 155 | 766 |

**Figure 30.—Time-weighted average resistance versus face distance for each shield.**

The cell pressure in the panel began to increase when the face was still 570 ft away. Of special interest is the sudden pressure increase resulting from the bump occurring on April 20, 1983, after 618 ft of advance, when the face was 330 ft away from the cell. The analysis of the data before and after this bump is presented because the bump occurred closest to the instrumented location. Postbump panel behavior (fig. 33) shows not only dramatic pressure increases, but also pressure redistribution. Panel stresses increased significantly from 20 to 40 ft inside the rib, while the cells installed at depths of less than 20 ft showed a pressure decrease. Reduction of the structural integrity and load-carrying ability of the panel edge is confirmed by rib expansion measurements shown in figure 34. Cumulative rib expansion was approximately 1.85 in at the collar and decreased with distance into the rib. Readings before and after the bump differed at the collar by 0.85 in and decreased with depth into the rib. Subsequent readings from this instrument were not possible because of the floor heave in the tailgate entry.

Because of the tailgate floor heave caused by the bump, access to areas ahead of the face was not permitted. This made

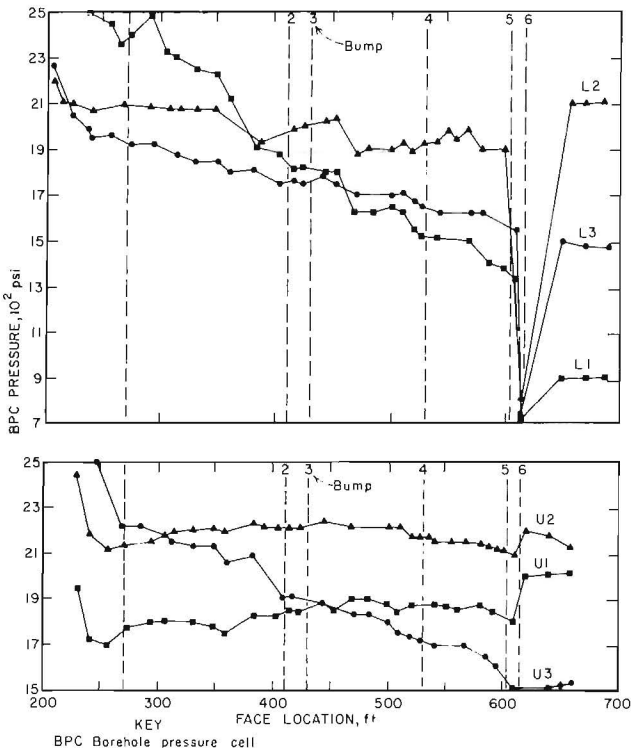


**Figure 31.—Pressure changes versus face location plots for upper and lower packwalls—dashed lines indicate bumps.**

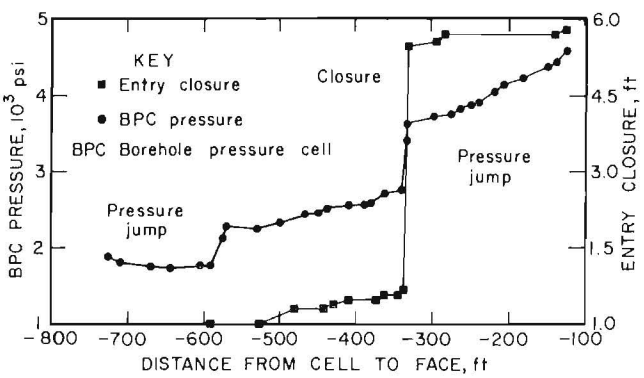


**Figure 32.—Pressure and entry closure versus distance from cell to face.**

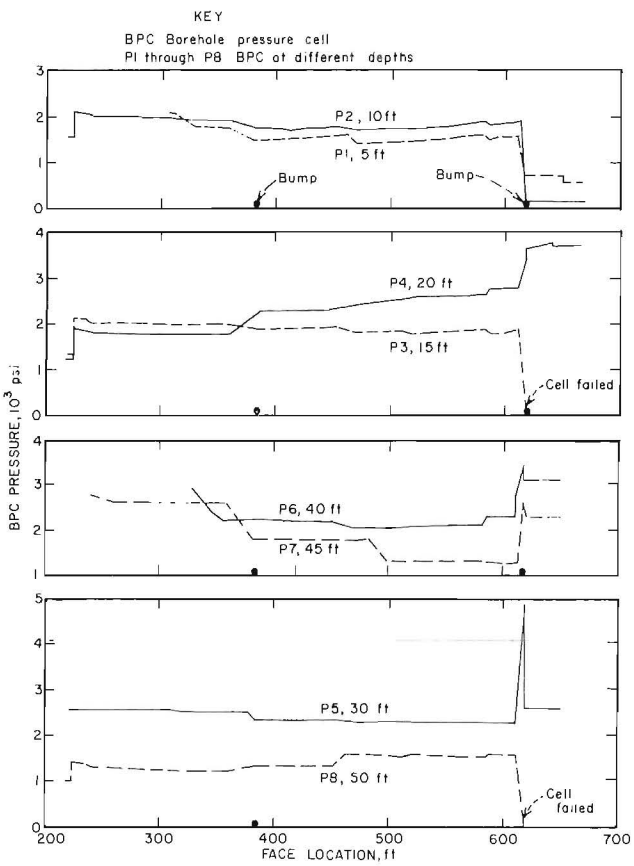


**Figure 33.—Pressure changes in panel at station 1 versus face position.**

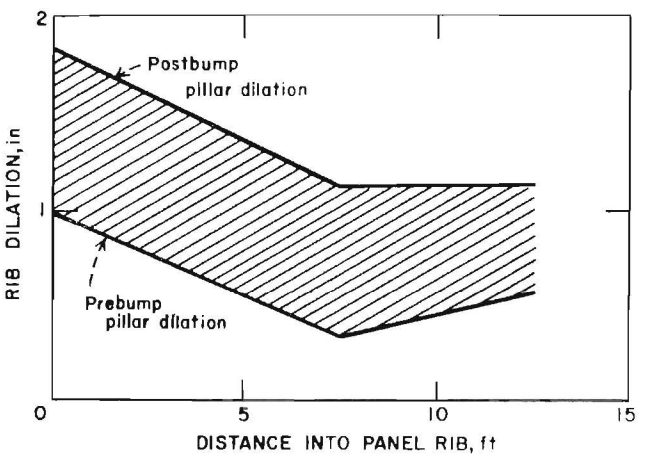


**Figure 34.—Panel rib dilation before and after April 20, 1983, bump.**

it difficult to further record data from station 2. However, subsequent readings indicated no bump effects on station 2 approximately 1,400 ft away from the bump location.

Figure 35 shows the difference in stress levels before and after a bump obtained from instruments in the panel at stations 1 and 2.

### Room Closure

Approximately 5 ft of roof-to-floor convergence at station 1 resulted from the April 20, 1983, bump. Convergence data from 10 other stations, located on 50-ft centers from 850 ft to 1,300 ft inby the starting room, indicated a mean forward abutment extent of 570 ft ahead of the face. Analysis of abutment-induced closure rate determined a mean closure rate of 0.004 ft/ft of advance, but did not provide any possible precursors to the major bump.

Similarly, roof-layer movement, obtained from the MPBX's located in the roof of the upper and lower entries of the tailgate at station 1, indicated a nearly uniform rate of immediate roof deflection with approach of the face. The roof layer separation versus face advance for three horizons above the coal seam are shown in figure 36.

As observed from the BPC data, the bump-induced pressure increase was accompanied by increased roof movement. Prebump roof deflection measurements indicated greater deflection for the lower roof beds than for the upper strata. Deflections in the upper entry usually exceeded lower entry roof movement. As the upper entry is adjacent to the previously mined gob and is further out under the cantilever beam extending from the panel toward the gob, greater roof deflection should be expected.

Data analysis obtained before and after the April 20, 1983, bump (fig. 37) indicates that floor failure may have centered about 80 to 100 ft inby the face. Floor failure may be due partially to the horizontal stress conditions, lack of roof caving and high abutment pressures, lateral loading from the previously mined longwall panel, or a combination of these and other factors.

## FAILURE MECHANISM

Conditions at this mine are very complex. Contributing factors include depth; strong roof in close proximity to the coal seam that apparently overhung behind the shields near the tailgate; lateral loading from the uphill, previously mined longwall panel; a floor comprised of a soft coalbed overlain by a strong shale-sandstone layer, which varies in thickness and is capable of storing strain energy; and a principal secondary horizontal stress component oriented approximately along the axis of the tailgate entries. While a detailed analysis is premature, the field data suggest a possible explanation for the April 20, 1983 bump that generally agrees with observed and measured behavior.

The forward abutment extended to approximately 570 ft ahead of the face with significant pressure increases occurring between 20 to 40 ft inside the panel rib. Abutment pressure increases consisted of two components: (1) a gradual increase associated with load transfer of the roof onto the panel and (2) two dynamic load increases that followed documented bump occurrences.

Superimposed onto the forward abutment loading is the effect of an apparent 145-ft-long cantilever roof beam extending behind the near-tailgate shields. Concurrent with the forward abutment loading is the lateral thrust from the

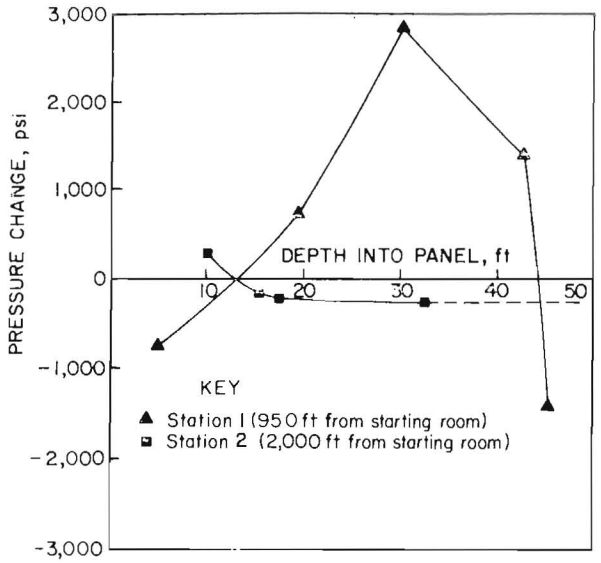


**Figure 35.—Pressure change from cells in panel at stations 1 and 2.**

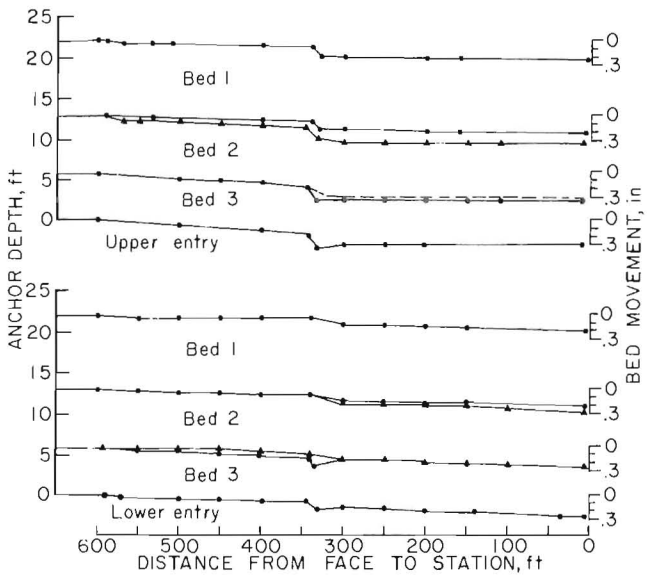


**Figure 36.—Roof-layer separation versus distance from face.**

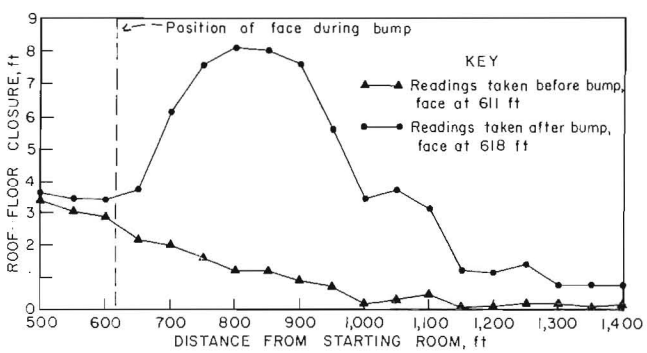


**Figure 37.—Roof-to-floor convergence versus distance from starting room before and after April 20, 1983, bump.**

previously mined panel onto the tailgate packwalls and panel rib. Lateral loading effects are most evident from roof deflection measurements that indicate roof inclination toward the previously mined gob and less evident from packwall pressure measurements. Prior to the bump on April 20, upper packwall pressures exceeded those measured in the lower packwall, but both revealed higher core pressures than near-rib pressures. Following the bump, the lower packwall lost pressure, while the upper one remained essentially undisturbed.

As entry closure measurements indicated that mining-induced convergence preceded the longwall face, a possible explanation for packwall behavior is presented. The shale-sandstone rock split is not only loaded by the horizontal stress field, the principal secondary components being oriented approximately along and normal to the entry axes, and combined forward and lateral abutments, but is also loaded from below by a soft, possibly plastic, coalbed. With approach of the face, floor movement from under the packwall ribs increased and contributed to decreases in packwall rib pressure.

The bump, after 618 ft of advance and presently conjectured as centered approximately 80 to 100 ft inby the face, imposed a sudden, dynamic load onto the already stressed tailgate entry. The ensuing bump resulted in a sudden uplift of the rock split and underlying coalbed. Destruction of the floor was accompanied by further dilation of the panel rib and panel rib pressure redistribution. Load-carrying capacity within 60 ft of the rib was generally lost, with the exception of a 20-ft-wide zone from 20 to 40 ft within the panel. This is explained by the yielding of the packwalls and the first 20 ft from the rib of the panel after the bump. Load transfer to other areas of the panel was not measured.

Postbump packwall response is apparently the result of the floor behavior. The lower packwall, adjacent to the heavily damaged lower tailgate entry, showed lower postbump pressures that may be explained as due to reduced bearing strength when the floor broke. The packwall essentially settled into the shattered floor debris. The upper packwall, somewhat confined by the adjacent gob and subjected to less floor heave in the upper tailgate entry, retained its prebump integrity and pressure levels. While some upper entry floor heave occurred, any pressure drops associated with heaving are believed to have been offset by the additional measured settling and rotation of the immediate roof onto this packwall. Postbump roof behavior suggests that the roof was supported by the upper packwall and also by the structurally competent 20-ft zone within the panel rib.

The April 20 bump is hypothesized as resulting from a complex combination of mining-induced and tectonic stresses, a hanging roof, and additional loading from the plastic flow of the lower coalbed. High vertical stress conditions resulted from overburden stress, additive forward and side abutments loads, and apparent cantilever effects. Lower coalbed deformation contributed to the floor failure by inducing additional flexure stresses within the rock split.

As critical pressure levels were reached, the floor violently failed, drastically reducing confinement to the panel and the bearing capacity of the packwall-floor components. Loss of confinement under the panel rib was accompanied by increased dilation and loss of structural integrity, as evident from the postbump panel pressure redistribution. Relationship between packwall behavior and floor heave is supported by convergence and pressure measurements, as detailed above.

Loading due to noncaving of the roof apparently contributed to the high-stress conditions; failure of the sandstone roof member may have imparted a sudden load onto the tailgate entries and panel. This preliminary analysis suggests that high stress, combined with dynamic loading, triggered the bump.

## RECOMMENDATIONS FOR MINING UNDER STRONG ROOF

As the longwall face advances, the roof layers behind the supports separate and cave. Depending on the geology, physical properties, and thickness of roof layers, the immediate roof may cave into the gob area immediately following the advance of the shields. The main roof breaks and falls periodically along the direction of the face advance and imposes periodic roof weighting (impact loads) on the face. Depending on the exposed roof length and the type of floor rock, the impacts may exert a dynamic loading to the shields and face. Consequently, the powered supports may be damaged because the impact loading occurs in a very short period of time, and the yielding valves do not react in time. If the floor rock is soft, the powered supports may sink into the floor under the roof pressure. This will reduce the supporting capacity of the shields and becomes a problem in advancing the supports. When the roof is thick, strong, and does not readily cave, it overhangs behind the powered supports and forms a cantilever beam extending into the gob; initially, the beam deflection is small, and no major increase in the abutment stress is noticed. However, as the face advances, the strong roof gradually overhangs for a long period of time or over a large span. Its weight, supported by the shields and face, causes the shield-leg pressure and the front-abutment stress to increase. When the stress in the coal exceeds the ability of the coal to store strain energy, a bump occurs.

Current methods, which address the problem of high-stress buildup in the face area, include detection and destressing of high-stress zones by volley firing, auger drilling, or hydraulic fracturing. Such methods have proven effective in reducing bump occurrences. After destressing the coal face, the structural integrity of the coal is lost, and the abutment stress is advanced ahead of the face; however, the immediate cause of the high-stress condition has not been removed. By destressing the face to a depth of 5 ft, for example, the length of the roof beam has increased by 5 ft. This condition adds loads to the shields and to the abutment in the coal panel 5 ft ahead of the current face. If the roof does not cave behind the shields by the time the face advances 5 ft and the face is destressed again, even more load is applied to the shields and panel. Eventually, the cantilever beam becomes so long and has stored so much energy that it fails; when the beam fails in this manner, a significant amount of load and energy has to go somewhere—to the shields, panel, etc.—and bumps may occur.

Another method, which was practiced at this mine, was destressing the floor ahead of the face in the tailgate entry. When the floor in the tailgate entry is destressed, the floor heaves, which causes the pillars or packwalls to sink or lose confinement. This causes the roof to sag toward the gob from a previously mined panel, and the load carried by the pillars or packwalls will be transferred to the panel and shields, which adds to the bump conditions.

From this study, correlation between bump conditions and caving of the roof was shown. A conclusion is that when the roof does not cave regularly, bump problems have been

recorded. The apparent solution is to induce regular caving in roof strata that do not readily cave.

There are two basic strategies to approach this problem: (1) increase shield setting pressures to fracture the roof, and/or (2) induce fracturing of the roof by some other means. European experiences with hydraulic fracturing have shown the beneficial effects of fracturing the roof strata over the coal seam ahead of the face (*36*). However, with hydraulic fracturing, it is difficult to control the extent of the fracture area; fracturing too large an area may create, rather than reduce, ground control problems. Another method (*42*) uses large-hole blasting to initiate the cave behind the shields. Depending on the roof thickness and rock physical properties, the hole specifications were as follows:

- Hole length = 13–23 ft,
- Hole diameter = 1.6–2.4 in,
- Inclination angle = 60°–65° from horizontal,
- Horizontal hole spacing = 20–33 ft,
- Distance from blast hole canopy = 1.3–2.0 ft.

A promising technique currently under investigation at the Bureau is the use of expansive grout, which was proven successful in fracturing large rocks without the use of explosives in the laboratory and in surface mines. The expansive-grout method uses lime compounds, which, when mixed with water and confined in a small borehole, generate expansive force of up to 9,000 psi by a chemical hydration reaction. The expansive force increases at a rate of 2,000 psi/d and allows fracturing to proceed without direct attention of workers. To create fractures in rock, holes may be located to act independently of each other or may be positioned so that the stresses from adjacent holes interact to generate cracks expanding from hole to hole along the line of the holes drilled. Required equipment includes a rock drill, small slurry pump, plugs to stopper filled holes, and tubing to bleed off air as holes are drilled. This method has the capability of fracturing rock without the disadvantages associated with blasting, such as noise and vibration, and it can be used in gassy mine environments without the added risks of explosives.

Even though induced caving may be an effective technique to control bumps in underground coal mines, many questions that require future research and field evaluation still exist:

a. Which available fracturing technique—blasting, hydrofracturing, or expansive grout—is most effective, given specific conditions in an underground coal mines?

b. What drilling pattern—hole size, length, spacing, and angle from horizontal—is most effective for each method?

c. How far should the hole be from the powered supports?

d. How does the thickness and strength of the roof rock influence the effectiveness of increasing the shield setting pressure? Can high shield setting pressure effectively fracture strong, thick roof rock?

e. What is the critical distance for the face to advance before inducing caving?

f. Does induced caving prove to be beneficial to conditions on the face and on the shields?

g. Which is more effective—induced fracturing of the roof *along the face* or *ahead of the face,* prior to mining?

Another method is to orient the long wall at 30° to the major fracture zone in the strong roof member. This allows the roof to break through the existing fractures.

## CONCLUSIONS

Four major parameters affect coal bumps and rock bursts: the ability of coal or rock to store and release strain energy, geologic characteristics, mine design, and physical properties of the coal and surrounding strata. Presently available sophisticated stress-detection methods cannot conclusively predict an impending rock burst. Since reliable prediction is nearly impossible, it may be more beneficial in bump-prone mines to use proper mine planning and inexpensive procedures to prevent or control stress buildup that may result in a bump rather than attempting to detect or predict a bump. The mine operator knows if the mine is bump prone. What is needed are methods to control or prevent the unpredicted bump. The hazard of an unplanned or unpredicted coal bump can be reduced by properly implemented volley firing, hydraulic fracturing, expansive grout fracturing, or auger drilling. The computer model results indicate that careless use of stress-relief methods may increase the potential for a coal bump on the face. Each area in different mines has site-specific characteristics that will indicate how ultimate stress-relief methods are to be used. Destressing the active face on a routine basis is recommended to move the abutment stress ahead of the face.

The case-study data analysis indicates that the bump on April 20, 1983, resulted from high forward abutment pressure compounded by noncaving of the strong sandstone roof layer. Shield-loading measurements, apparently the best indicator of abnormal conditions, revealed that while the headgate and center portion of the face underwent periodic weightings, the near-tailgate face area experienced a substantial period of high loading prior to the bump. While the exact cause of the bump is unknown, contributing factors include a combination of high local stresses and the presence of strong roof and floor. Floor heave in the tailgate caused loss of confinement of the pillars or packwalls, and the load carried by these pillars was transferred to the panel, which added to the bump conditions.

Closure data suggest that the bump centered on an area 80 to 100 ft ahead of the face, but discrete closure and closure-rate measurements did not provide any indicators, precursors, to the event.

Even though current techniques to detect and destress high stresses in the face area have proven effective to control bumps during face advance, they do not eliminate the basic cause of the high stress: the ability of strong, near-seam strata to accumulate strain energy. A promising technique is the use of expansive grout to induce controlled caving without the use of explosives. Induced fracturing may be an effective bump-control technique; however, many questions that require further research and field evaluation still exist.

## REFERENCES


1. Phillips, W. Rock Bursts and Bumps in Coal Mines. Trans. Inst. Min. Eng., v. 104, 1944, pp. 55-94.

2. _____. Tectonics in Mining. Colliery Eng., 1948, pp. 1-12.

3. Holland, C.T., and E. Thomas. Coal Mine Bumps—Some Aspects of Occurrence, Cause, and Control. BuMines B 535, 1954, 65 pp.

4. Zanski, J. Podziemna Eksploalogia. Zloc. Katowice, 1964, 8 pp. (Engl. trans.).

5. Spalding, J. Deep Mining. Min. Publ. Ltd., London, 1948, 14 pp.

6. Cook, N. W. The Basic Mechanics of Rock Bursts. J. S. Afr. Inst. Min. and Metall., Dec. 1963, pp. 192-195.

7. Neyman, B., A. Szecowka, and W. Zuberek. Effective Methods for Fighting Rock Bursts in Polish Collieries. Fifth Int. Strata Control Conf. 1972, 9 pp. (preprint).

8. Weiss, O. Causes of Rock Bursts. J.S. Afr. Inst. Min. and Metall., Oct. 1942, pp. 103-107.

9. Holland, C. T. Rock Burst or Bumps in Coal Mines. Colliery Eng., Apr. 1955, pp. 145-153.

10. Adler, L., and M. Sun. Ground Control in Bedded Formations. VA Tech. Bull. 28, 1976, 268 pp.

11. Lama, R. D. Some Aspects on Planning of Deposits Liable to Rock Bursts. J. Mines, Met., and Fuels, May 1967, pp. 149-158.

12. Campbell, W. F. Deep Coal Mining in Spring Hill No. 2 Mine. Trans. Soc. Min. Eng. AIME, Sept. 1958, pp. 987-992.

13. Perkin, J. Mountain Bumps at Sunnyside Colliery. Min. Eng. (v. 10, no. 9), 1958, pp. 562-582.

14. Hackett, P. Rock Bursts. Colliery Guardian, Aug. 1962, pp. 421-433.

15. Mohr, F. Rock Pressure and Mine Support. Mine and Quarry Eng., June 1956, pp. 215-237.

16. Miard, H. E. Sudden Release of Ground Stresses in Coal Mines of Western Canada. Joint Advisory Committee Conf. on Outbursts of Coal and Firedamp. Oct. 5, 1965, 10 pp.

17. Obert, L., and W. Duvall. Microseismic Method of Predicting Rock Failure in Underground Mining. BuMines RI 3797, 1945, 14 pp.

18. Herd, W. Bumps in No. 2 Mine, Springhill, Nova Scotia. Trans. Can. Inst. Min. and Metall., v. 32, 1929, pp. 413-457.

19. Rice, G. S. Bumps in the Coal Mines of the Cumberland Field, Kentucky and Virginia—Causes and Remedy. BuMines RI 3267, 1935, 27 pp.

20. Kripakov, N. P., L. A. Beckett, and D. A. Donato. Loading on Mine Structures Influenced by Multiple Seam Interactions. Paper in the Proceedings of the International Symposium on Application of Rock Characterization Techniques in Mine Design, ed. by M. Karmis (Soc. Min. Eng. AIME Annu. Meet., New Orleans, LA, Mar. 1986). Soc. Min. Eng. AIME, 1986, pp. 225-235.

21. Babcock, C. O., and D. Bickel. Constraint—The Missing Variable in the Coal Burst Problem. Paper in Proceedings of 25th Symposium on Rock Mechanics, ed. by C. H. Dowding and M. M. Singh (cosponsored by Northwestern Univ. and U.S. Natl. Comm. on Rock Mech., Evanston, IL, June 25-27, 1984), Soc. Min. Eng. AIME, 1984, pp. 539-647.

22. Fajklewicz, Z. Rock Burst Forecasting and Genetic Research in Coal Mines by Microgravity Method. Forecasting Rock Bursts, Geophysics, Proc., v. 31, 1983, pp. 748-765.

23. Grabis, Z., Z. Hladysz, and A. Kidybinski. Rock Bursts. Mining Hazards, 1976, pp. 32-35.

24. Anticipating Rock Bursts by Photoelastic Methods. New Sci., v. 363, Dec. 1963, pp. 605-608.

25. Spokane Daily Chronicle. Small Device May Detect Rock Bursts. June 1976, p. 1.

26. Oyler, D. C., and A. A. Campoli. Factors Influencing the Occurrence of Coal Pillar Bumps at the 9-Right Section of the Olga Mine. Paper in the Proceedings Sixth International Conference on Ground Control in Mining, ed. by S. S. Peng (cosponsored by BuMines, MSHA, and WV Univ., Morgantown, WV, June 9-11, 1987). Dep. Min. Eng., Coll. of Miner. and Energy Resour., WV Univ., Morgantown, WV, 1987, pp. 10-17.

27. Obert, L. and W. Duvall. Rock Mechanics and the Design of Structures in Rock. Wiley, 1967, 650 pp.

28. Jackson, L. J. Outbursts in Coal Mines. IEA Coal Research, London, Rep. ICTIC/TR2S, 1984, 55 pp.

29. McCabe, W. M. Acoustic Emission in Coal: A Laboratory Study. Paper in Second Conference on Acoustic Emission/Microseismic Activity in Geologic Structures and Materials, ed. by H. R. Hardy, Jr., and F. W. Leighton (Proc. Conf. PA State Univ., University Park, PA, Nov. 13-15, 1978). Clausthal-Zellerfeld, Fed. Repub. Germany, Trans. Tech. Publ. D-3392, 1980, pp. 35-51.

30. Blake, W., F. Leighton, and W. Duvall. Microseismic Techniques for Monitoring the Behavior of Rock Structures. BuMines B. 665, 1974, 65 pp.

31. Chugh, V., and G. Heidinger. Effect of Coal Lithology on Observed Microseismic Activity During Laboratory Tests. Paper in Second Conference on Acoustic Emission/Microseismic Activity in Geologic Structures and Materials, ed. by H. R. Hardy, Jr., and F. W. Leighton (Proc. Conf. PA State Univ., University Park, PA, Nov. 13-15, 1978). [Trans. Tech. Publ. D-3392 Clausthal-Zellerfeld Federal Republic of Germany, 1980, pp. 55-61.]

32. Blake, W. Microseismic Applications for Mining—A Practical Guide (contract J0215002). BuMines OFR 52-83, 1983, 206 pp.; NTIS PB 83-180877.

33. Varley, F. D. Outburst Control in Underground Coal Mines. Paper in the Proceedings of the Fifth Conference on Ground Control in Mining, ed. by A. Wahab Khair and S. S. Peng (cosponsored by BuMines, MSHA, and WV Univ., Morgantown, WV, June 11-13, 1986). Dep. Min. Eng., Coll. Miner. and Energy Resour., WV Univ., Morgantown, WV, 1986, pp. 249-256.

34. Haramy, K. Y., K. Hanna, and J. P. McDonnell. Investigations of Underground Coal Mine Bursts. Paper in the Proceedings of the Fourth Conference on Ground Control in Mining, ed. by S. S. Peng and J. H. Kelley (cosponsored by BuMines, MSHA, and WV Univ., Morgantown, WV, July 22-24, 1985). Dep. Min. Eng., Coll. Miner. and Energy Resour., WV Univ., Morgantown, WV, 1985, pp. 127-134.

35. Coeuillet, R. Coal and Gas Outbursts. Paper in Proceedings of Symposium on Coal and Gas Outbursts, Economic, (Nimes, France), 1964, pp. 1-14.

36. Sikora, W., A. Kidybinski, and K. Saltysek. Designing of Hard Roof-Rock Destressing Systems for Safe Warning of Rock Burst Prone Coal Seams, Central Mining Institute Report, Poland, 1978, 26 pp.

37. Talman, W. G., and J. L. Shrooder. Control of Mountain Bumps in the Pocahontas No. 4 Seam. Trans. Soc. Min. Eng. AIME, v. 211, 1958, pp. 888-891.

38. Haramy, K., J. McDonnell, and L. Beckett. Stress Relief to Control Coal Bursts. Soc. Min. Eng. AIME Preprint 87-57, 1987, 12 pp.

39. Sinha, K. P. Displacement Discontinuity Technique for Analyzing Stresses and Displacements Due to Mining in Seam Deposits. Ph. D. Thesis, Univ. MN, Minneapolis, MN, 1979, 310 pp.

40. Haramy, K. Y. Borehole Shear Tester: Equipment and Technique, BuMines IC 8867, 1981, 19 pp.

41. Haramy, K.Y., and M.J. DeMarco. Use of the Borehole Shear Tester in Pillar Design. Paper in Proceedings of the 24th U.S. Symposium on Rock Mechanics, ed. by C. C. Mathewson (cosponsored by Texas A&M Univ., Assoc. of Eng. Geol. and U.S. Natl. Acad. Sci. Natl. Res. Coun., College Station, TX, June 20-23, 1983). Assoc. Eng. Geol., 1983, pp. 639-644.

42. Peng, S.S., and H.S. Chiang. Longwall Mining, Wiley, N.Y., 1984, 708 pp.

# APPENDIX.— TURMAG DRILL MODEL "FORTSCHRITT III"[1]

The Turmag drill model "Fortschritt III" was designed to accurately and rapidly drill 32- to 145-mm-diam holes in coal for lengths up to 30 m. The drill is lightweight, operates at low noise, and has variable speeds. Drill specifications are listed in table A-1.

The low-cost West German drill is equipped with the following:

- Integral, maintenance-free overload protection, which, in case of jamming, will retain the operating torque and prevent an undesirable increase of the torque applied.
- Load-dependent speed control to protect the material and to reduce noise levels.
- Integral, maintenance noise abatement system without danger of contamination and capacity reduction with a noise emission level of less than 92 dB.
- A steel housing that protects all components and assures longer life.
- Handy grips on opposite sides of the center of gravity of the machine.

[1]Reference to specific equipment does not imply endorsement by the Bureau of Mines.

**Table A-1.—Technical information on the Fortschritt III auger drill**

| | |
|---|---|
| Borehole diameter | 1.3 to 5.7 in. |
| Borehole depth | 984 ft. |
| Forward feed system | Manual. |
| Drill rate | 1 to 16.5 ft/min. |
| Drive power | 1.7 × $10^{-3}$ Btu/s. |
| Drilling speed | 600 to 1,000 min. |
| Torque | 2,164 lb·ft (at 600 rpm). |
| Air consumption | 22.2 lb·$ft^3$/min. |
| Flushing water consumption | 1.3 to 6.6 U.S. gal/min. |
| Drill weight | 27.6 lb. |
| Drill length | 14.0 in. |
| Drill width | 22.6 in. |
| Drill height | 6.3 in. |
| Air connection | 0.7-in-ID hose. |
| Connecting threads | 32 by 1/8 in. |
| Overload protection | Integral. |
| Noise emission | Less than 92 dB. |
| Operating pressure | 58 psi. |
| Drill bits used | 13.2- to 2.0-in diam. |
| Drill rods used | 1.1-in diam. |

☆ U.S. GOVERNMENT PRINTING OFFICE: 611-012/00,030

INT.-BU. OF MINES, PGH., PA. 28864